

# Masses of galaxy clusters from gravitational lensing

Henk Hoekstra · Matthias Bartelmann ·  
 Håkon Dahle · Holger Israel · Marceau  
 Limousin · Massimo Meneghetti

Received: date / Accepted: date

**Abstract** Despite consistent progress in numerical simulations, the observable properties of galaxy clusters are difficult to predict ab initio. It is therefore important to compare both theoretical and observational results to a direct measure of the cluster mass. This can be done by measuring the gravitational lensing effects caused by the bending of light by the cluster mass distribution. In this review we discuss how this phenomenon can be used to determine cluster masses and study the mass distribution itself. As sample sizes increase, the accuracy of the weak lensing mass estimates needs to improve accordingly. We discuss the main practical aspects of these measurements. We review a number of applications and highlight some recent results.

**Keywords** Clusters of galaxies · Gravitational lensing · Cosmology

## 1 Introduction

Inhomogeneities in the matter distribution perturb the paths of photons that are emitted by distant galaxies. The result is equivalent as if we are viewing these sources through a piece of glass with a spatially varying index of refraction: the images appear slightly distorted and magnified. Both effects can be measured in principle, and can be used to determine (projected) masses, because the amplitude of the distortion provides

---

H. Hoekstra  
 Leiden Observatory, Leiden University, Leiden, The Netherlands

M. Bartelmann  
 Zentrum für Astronomie, Institut für Theoretische Astrophysik, Heidelberg, Germany

H. Dahle  
 Institute of Theoretical Astrophysics, University of Oslo, Oslo, Norway

H. Israel  
 Argelander-Institut für Astronomie, Bonn University, Bonn, Germany

M. Limousin  
 Laboratoire d'Astrophysique de Marseille, Aix Marseille Université, CNRS, Marseille, France

M. Meneghetti  
 INAF - Osservatorio Astronomico di Bologna, Bologna, Italy &  
 INFN, Sezione di Bologna, Bologna, Italy

a direct measure of the gravitational tidal field, independent of the nature of the dark matter or the dynamical state of the system of interest. This is particularly useful for clusters of galaxies, which are dynamically young and often show signs of merging.

If the deflection of the light rays is large enough, multiple images of the same source can be observed: these strong lensing events provide precise constraints on the mass on scales enclosed by these images. This phenomenon was already discussed by Zwicky (1937), but the first observation was made more than 40 years later with the discovery of a gravitationally lensing QSO (Walsh et al. 1979). The discovery of strong lensing by a cluster of galaxies was reported by Soucail et al. (1987), and is now seen routinely, in particular in deep observations with the *Hubble Space Telescope*. The study of strong lensing systems has a number of applications, which are discussed in Bartelmann et al. (2012); Meneghetti et al. (2012). In this review we limit the discussion to the use of strong lensing to determine masses of galaxy clusters. Unfortunately, the effect is confined to the inner regions, and comparison with other proxies for mass requires extrapolation to larger radii.

The lensing effect itself, however, is not limited to small scales. At large radii the tidal field causes a subtle change in the shapes of galaxies, resulting in a coherent alignment of the sources that can be measured statistically. As the signal is proportional to the mass of the system, galaxy clusters were the first objects to be studied using this weak gravitational lensing technique, with the first detection of the signal presented by Tyson et al. (1990). The '90s saw a rapid development of the field, and a shift from studying clusters of galaxies to the statistical properties of the large-scale matter distribution: the cosmic shear (see e.g., Hoekstra & Jain 2008, for a review). The latter application was made possible thanks to the advent of mosaic cameras on large telescopes, but also led to improved methods to measure the shapes of galaxies. In addition, the desire to study the lensing signal as a function of redshift has improved our knowledge of the source redshift distribution, which is needed to convert the lensing signal into an actual mass. This progress over the past 20 years has also benefited the work on clusters of galaxies, which now can be studied out to larger radii, and with improved accuracy.

Here we provide a brief introduction how the observable consequences of gravitational lensing can be used to determine masses of galaxy clusters, with a focus on a number of practical aspects. We contrast the advantages (and disadvantages) of both strong and weak lensing and discuss some recent results. The principles of gravitational lensing are briefly reviewed in §2, but readers interested in lensing results can skip this, as well as §3 where we discuss some of the technical issues arising in the measurement and interpretation of the weak lensing signal. Some highlights of mass reconstructions are reviewed in §4 and a discussion of the properties of cluster halos, such as density profiles and halo shapes, can be found in §5. Cluster mass estimates are discussed in §6 and some measurements of the halos of cluster galaxies are presented in §7. We conclude and present an outlook in §8.

## 2 Gravitational lensing

We start with a basic introduction of gravitational lensing, with a particular focus on applications that pertain to clusters of galaxies. We refer the interested reader to more thorough introductions into the subject by Bartelmann & Schneider (2001), Schneider (2006) or Bartelmann (2010).

As mentioned in the introduction, inhomogeneities along the line-of-sight deflect photons that are emitted by distant galaxies (the sources). As a result a source with a true position  $\beta$  is actually observed at positions  $\mathbf{x}$  that satisfy the lens equation

$$\beta = \mathbf{x} - \alpha(\mathbf{x}), \quad (1)$$

where  $\alpha$  is the deflection angle (see Fig. 11 in Bartelmann & Schneider 2001, for a diagram). Note that the lens equation can have multiple solutions for  $\mathbf{x}$ , which means that several images of the same source are observed. The case when multiple images are produced is commonly referred to as “strong gravitational lensing”. As discussed in §2.1, this phenomenon can be used to provide very precise constraints on the mass distribution in cluster cores (also see Meneghetti et al. (2012) in this volume).

An important feature of gravitational lensing is that it conserves the surface brightness: for a source with a true surface brightness distribution  $f^s(\mathbf{x})$  the observed surface brightness distribution is given by

$$f^{\text{obs}}(\mathbf{x}) = f^s[\beta(\mathbf{x})]. \quad (2)$$

Away from the lens, where the deflection angle as well as its spatial variation are typically small compared to the extent of the source, this mapping can be linearized. This case is commonly referred to as “weak gravitational lensing”, and the resulting remapping of the surface brightness distribution can be written as

$$f^{\text{obs}}(x_i) = f^s(\mathcal{A}_{ij}x_j), \quad (3)$$

where  $\mathbf{x}$  is the position on the sky and  $\mathcal{A}$  is the distortion matrix (i.e., the Jacobian of the transformation), which is specified by the projected surface density of the lens and the redshifts of the lens and the source. It is convenient to introduce the deflection potential  $\Psi$

$$\Psi(\mathbf{x}) = \frac{1}{\pi} \int d^2\mathbf{x}' \kappa(\mathbf{x}') \ln |\mathbf{x} - \mathbf{x}'|, \quad (4)$$

where the convergence  $\kappa$  is the ratio of the projected surface density  $\Sigma(\mathbf{x})$  and the critical surface density  $\Sigma_{\text{crit}}$ :

$$\kappa(\mathbf{x}) = \frac{\Sigma(\mathbf{x})}{\Sigma_{\text{crit}}}, \quad (5)$$

with  $\Sigma_{\text{crit}}$  defined as

$$\Sigma_{\text{crit}} = \frac{c^2}{4\pi G} \frac{D_s}{D_l D_{ls}}. \quad (6)$$

Here  $D_s$ ,  $D_l$ , and  $D_{ls}$  correspond to the angular diameter distances between the observer and the source, observer and the lens, and the lens and the source. Hence, the lensing signal depends on the redshifts of both the lenses and the sources. The implications of this are discussed in more detail in Section 3.2.

The distortion matrix  $\mathcal{A}$  can be written in terms of the second derivatives of the deflection potential  $\Psi$

$$\mathcal{A} = \delta_{ij} - \frac{\partial^2 \Psi}{\partial x_i \partial x_j} = \begin{pmatrix} 1 - \kappa - \gamma_1 & -\gamma_2 \\ -\gamma_2 & 1 - \kappa + \gamma_1 \end{pmatrix} = (1 - \kappa) \begin{pmatrix} 1 - g_1 & -g_2 \\ -g_2 & 1 + g_1 \end{pmatrix}, \quad (7)$$

where we used that  $2\kappa = \nabla^2\Psi$ , introduced the complex shear  $\gamma \equiv \gamma_1 + i\gamma_2$ , and defined the reduced shear  $g_i = \gamma_i/(1 - \kappa)$ . The shear is related to the deflection potential through

$$\gamma_1 = \frac{1}{2} \left( \frac{\partial^2\Psi}{\partial x_1^2} - \frac{\partial^2\Psi}{\partial x_2^2} \right) \quad \text{and} \quad \gamma_2 = \frac{\partial^2\Psi}{\partial x_1 \partial x_2}, \quad (8)$$

The effect of the remapping by  $\mathcal{A}$  is to transform a circular source into an ellipse with axis ratio  $\sim (1 - |g|)/(1 + |g|)$  and position angle  $\alpha = \arctan(g_2/g_1)/2$ ; the reduced shear describes the anisotropic distortion of a source. If  $\kappa \ll 1$  (i.e., the weak lensing regime), the observable  $g_i \sim \gamma_i$ . In addition, the source is magnified by a factor

$$\mu = \frac{1}{\det \mathcal{A}} = \frac{1}{(1 - \kappa)^2 - |\gamma|^2} = \frac{1}{(1 - \kappa)^2(1 - |g|^2)}, \quad (9)$$

boosting the flux by the same amount. To first order, the magnification depends on the convergence only; i.e.  $\kappa$  describes the isotropic distortion of a source (contraction or dilation). Both the shearing and magnification of sources are observable effects, although both are quite different in terms of techniques and systematics.

Note that the shear and convergence are related to one another through the deflection potential. As a result it is possible to express the shear as a convolution of the convergence with a kernel  $\chi(\mathbf{x})$ . This can be seen by computing the shear following Eqn. 8, starting from Eqn 2:

$$\gamma(\mathbf{x}) = \frac{1}{\pi} \int d^2\mathbf{x}' \chi(\mathbf{x} - \mathbf{x}') \kappa(\mathbf{x}'), \quad (10)$$

where the convolution kernel  $\chi(\mathbf{x})$  is given by

$$\chi(\mathbf{x}) = \frac{x_2^2 - x_1^2 - 2ix_1x_2}{|\mathbf{x}|^4}. \quad (11)$$

As first shown by Kaiser & Squires (1993), this expression can be inverted, i.e. it is possible to express the surface density in terms of the observable shear:

$$\kappa(\mathbf{x}) - \kappa_0 = \frac{1}{\pi} \int d^2\mathbf{x}' \chi^*(\mathbf{x} - \mathbf{x}') \gamma(\mathbf{x}'), \quad (12)$$

where the constant  $\kappa_0$  shows that the surface density can only be recovered up to a constant, and reflects the fact that a constant  $\kappa$  does not cause a shear. In fact one can show that a transformation  $\kappa' = \lambda\kappa + (1 - \lambda)$  leaves the reduced shear unchanged. This is known as the mass-sheet degeneracy (Gorenstein et al. 1988). The possibility to reconstruct the surface mass density is an important application of weak gravitational lensing, which is discussed in more detail in §4. Note that  $\kappa(\mathbf{x})$  is a real function, but that the reconstruction in principle can have an imaginary part as well. This can be used to examine fidelity of the mass map and may help identify issues with the analysis of the data (see §3.1).

## 2.1 Strong gravitational lensing

Strong gravitational lensing and its applications to galaxy clusters are discussed in detail in a dedicated contribution to this volume (Meneghetti et al. 2012). Here we give a brief introduction and refer the interested reader to the separate review for further information.

Several different meaningful definitions of strong lensing are possible and are being used. In the context of galaxy clusters, we define gravitational lenses as strong if they are capable of producing multiple images from single sources. For this to happen, the lens mapping must become locally multiply defined, which means that the Jacobian matrix  $\mathcal{A}$  of the lens mapping must be singular somewhere:

$$\det \mathcal{A}(\mathbf{x}_c) = 0. \quad (13)$$

The set of angular positions  $\mathbf{x}_c$  on the sky where Eqn. 13 is satisfied can be shown to form closed curves, which are called critical curves. Their images  $\beta_c$  under the lens mapping are called caustics. A sufficient, but not necessary condition for a gravitational lens to be strong, or synonymously to become supercritical, is that its surface-mass density  $\Sigma$  exceeds the critical value  $\Sigma_{\text{crit}}$  at least somewhere within the lens. Where this happens, the convergence exceeds unity, i.e.  $\kappa > 1$ .

Sources near caustics are strongly distorted. Multiple images form in pairs as sources cross caustics inward. Since a source very far away from the lens must have a single image, the number of images produced by gravitational lenses must thus be odd, unless the lens has a singular lensing potential. Caustic points with well-defined tangents are called fold points, others (“tips”) are called cusp points. If a source approaches a fold point or a fold section from within a caustic, two of its images approach from either side of the corresponding section of the critical curve, merge once the source crosses the caustic outward and disappear as the source moves on. For sources approaching cusp points from the inside out, three of their images approach and merge to form a single, strongly distorted and highly magnified image. The largest gravitational arcs, which are the perhaps the most impressive manifestations of strong lensing by galaxy clusters, are often formed from sources near cusp points.

Typically, two caustics or critical curves may be formed in a strong lens, one for each of the two eigenvalues of the Jacobian matrix of the lens mapping. They are distinguished by the preferential orientation of the distortions experienced by sources near these caustics. If two caustics are formed, typically the inner one is mapped to the outer critical curve, where images appear tangentially distorted relative to the lens’ center. These curves are called the tangential caustics or critical curves. Sources near the other caustic, usually mapped to the inner critical curve, are imaged in a radially distorted fashion. The respective caustics and critical curves are hence called radial. Radially distorted images, commonly called radial arcs, are often hard to recognise since they occur very close to cluster centers where they are often outshone by bright, central cluster galaxies. Where they can be found, they provide important constraints on the local slope of the density profile.

The importance of strong cluster lensing and of the critical curves is most easily illustrated with axially-symmetric lens models, even though they certainly are not the most realistic. Such lenses can be characterised by the dimensionless mass  $m(r)$

$$m(r) = 2 \int_0^r r' dr' \kappa(r'), \quad (14)$$

where the radius  $r = |\mathbf{x}|$ . In axially-symmetric lenses, radial critical curves occur where

$$\frac{d}{dr} \frac{m(r)}{r} = 1, \quad (15)$$

while tangential critical curves require

$$m(r) = r^2. \quad (16)$$

The second relation immediately provides an estimate for the cluster mass enclosed by a tangential critical curve at radius  $r_t$ . Multiplying with  $\pi D_l^2 \Sigma_{\text{crit}}$  converts the dimensionless mass  $m(r_t)$  on the left-hand side to the projected mass enclosed by the physical radius  $D_l r_t$  and gives

$$M(\theta_t) = \pi D_l^2 r_t^2 \Sigma_{\text{crit}} \approx 4.4 \times 10^{14} M_\odot \left( \frac{r_t}{30 \text{ arcsec}} \right)^2 \left( \frac{D_l D_s}{D_{\text{ls}} \text{ Gpc}} \right). \quad (17)$$

This simple relation is the basis for cluster mass estimates based on strong gravitational lensing. The location of the critical curve can be determined relatively well (especially compared to weak lensing measurements). As a consequence the estimate of the projected mass is precise, but not necessarily accurate as a caveat concerning estimates obtained from (Eqn. 17) should be mentioned. Equations (14) and (16) together imply that the mean convergence within a tangential critical circle is unity for axially-symmetric lenses. Under very general conditions, it can be shown that realistic tangential critical curves enclose a lower mean convergence. In simulated, asymmetric clusters, tangential critical curves were found to enclose a mean convergence of  $\approx 0.82$ , while circles around cluster centers traced by tangential arcs enclose a mean convergence of only  $\approx 0.65$  (Bartelmann 1995). This systematic bias in cluster mass estimates based on axially-symmetric models is due to the fact that at fixed mass, the stronger gravitational tidal field of an asymmetric mass distribution increases the extent of the critical curves.

More accurate mass estimates require detailed modelling of the observable effects of strong lensing, either arcs or multiple images. On galaxy cluster scales, this is commonly done via the so-called *parametric* approach (e.g. Kneib et al. 1996; Broadhurst et al. 2005). It consists of building up a model for the lensing cluster by combinations of different potentials,

$$\psi = \sum_i \psi_i(\mathbf{p}). \quad (18)$$

Each potential is characterized by a set of parameters, defining for instance the radial scaling of  $\psi_i$ , its ellipticity and orientation, and its position. All these parameters are encoded in the general vector  $\mathbf{p}$  in the above formula. The parameters are varied trying to fit the observed strong lensing features. To quantify the goodness of the fit one defines  $\chi^2$  variables, either in the lens and/or in the source plane, to compare the observed and the predicted properties of the strong lensing features. The best fit model is obtained by minimizing the  $\chi^2$ . For example, if a set of  $n_i$  multiple images at the positions  $\mathbf{x}_{\text{obs}}^{ij}$  is used to build the lens model, one can define the  $\chi_i^2$  on the lens plane

$$\chi_i^2 = \sum_{j=1}^{n_i} \frac{[\mathbf{x}_{\text{obs}}^{ij} - \mathbf{x}^{ij}(\mathbf{p})]^2}{\sigma_{ij}^2}, \quad (19)$$

where we have denoted with  $\mathbf{x}^{ij}(\mathbf{p})$  the position of the image  $j$  of the multiple system  $i$  predicted by the model for the set of parameters  $\mathbf{p}$ , while  $\sigma_{ij}$  is the associated position error. If  $n$  sets of multiple images are available, the contributions to the total  $\chi^2$  by each set  $i$  are summed:

$$\chi^2 = \sum_i \chi_i^2. \quad (20)$$

Defining a  $\chi^2$  on the source plane is slightly more complicated. Let us consider the multiple image system  $i$ . For each image  $\mathbf{x}_{\text{obs}}^{ij}$ , the current lens model will predict a source at  $\mathbf{y}^{ij}(\mathbf{p})$ . If we impose that all multiple images originate from the same source, which we assume to be located at  $\hat{\mathbf{y}}^i(\mathbf{p}) = 1/n_i \sum_{j=1}^{n_i} \mathbf{y}^{ij}(\mathbf{p})$ , we can define the  $\chi^2$  on the source plane as

$$\chi_{S,i}^2 = \sum_{j=1}^{n_i} \frac{[\mathbf{y}^{ij}(\mathbf{p}) - \hat{\mathbf{y}}^i(\mathbf{p})]^2}{\sigma_{ij}^2 \mu_{ij}^{-2}}. \quad (21)$$

Note that the position error on the source plane has been obtained by correcting the position error on the lens plane by the magnification factor  $\mu_{ij}$ .

In the construction of the model it is important to include the contributions from all the relevant mass components of the lens. One or more smooth large scale components, resembling the cluster dark matter halo, are generally combined with smaller scale perturbers. These are typically associated with the bright galaxies in the cluster. Due to the complexity of the systems if each perturber is optimized individually, the number of free parameters in the model can rapidly saturate. To avoid this, a common practice is to vary the strength of all perturbers simultaneously using scaling relations (e.g. Jullo et al. 2007). As discussed in §7, this can be used to also constrain the properties of the halos of cluster galaxies.

Meneghetti et al. (2010) tested the robustness of parametric strong lensing modeling techniques using simulated observations of galaxy clusters. They found that the mass is very well constrained around the cluster critical lines, i.e. where the multiple image systems that are used to optimize the model are located. The typical accuracy achieved on the mass determination within the Einstein radius is  $\sim 5\%$ . However, the recovered mass profiles can deviate significantly from the true profile away from the critical lines. Since these typically extend to  $\lesssim 100$  kpc, which is smaller than the scale radius of a massive cluster-scale dark-matter halo, strong lensing alone cannot robustly measure the concentration of the lenses, unless it is combined with weak lensing data.

*Flexion:* The study of the transition from the strong lensing regime to the small weak lensing distortions has recently been developed. In this regime the galaxies are no longer multiply imaged, but the variation of the shear across the source itself cannot be ignored: the higher order terms in the expansion of the distortion matrix become important. As a result the galaxies appear somewhat skewed and "banana"-shaped (e.g., Goldberg & Natarajan 2002; Goldberg & Bacon 2005; Irwin & Shmakova 2005; Bacon et al. 2006). This can be measured and provides additional information, compared to the shear alone (e.g., Leonard et al. 2007; Okura et al. 2008; Leonard & King 2010).

Whereas the shear measures a density contrast which can be used to determine masses, the measurement of the flexion signal is mostly sensitive to the gradient of the density distribution. Furthermore, it requires a substantial spatial variation of the shear field. Consequently, the flexion signal is most suited for the study of the density

profiles and substructure in the inner regions of galaxy clusters. It is therefore discussed in more detail in Bartelmann et al. (2012).

## 2.2 Weak gravitational lensing

In the case of weak gravitational lensing the changes in the observable properties of the galaxies are more subtle, and the measurement of the lensing signal requires an ensemble of sources. Compared to strong lensing studies, the statistical nature of weak lensing limits the precision with which masses can be determined. This shortcoming is, however, in part compensated by the fact that any density fluctuation causes a distortion of the gravitational tidal field. The resulting signal can therefore be measured, provided the surface density of sources is high enough. Furthermore, as is discussed in more detail in §4, it is possible to reconstruct an image of the matter distribution.

When  $\kappa$  and  $\gamma$  are small, the effect of gravitational lensing is to change the unlensed ellipticity of a galaxy,  $\epsilon_{\text{orig}}$  (defined as  $(a - b)/(a + b)$ , where  $a$  is the semi-major axis, and  $b$  the semi-minor axis) to an observed value:

$$\epsilon^{\text{obs}} = \frac{\epsilon^{\text{orig}} + g}{1 + g^* \epsilon^{\text{orig}}} \approx \epsilon^{\text{orig}} + \gamma, \quad (22)$$

where the asterisk denotes the complex conjugate. Only if the shear is larger than  $\epsilon^{\text{orig}}$  does the observed ellipticity of a single galaxy provide a useful estimate of the shear. A population of intrinsically round sources would therefore be ideal. In practice galaxies have an average intrinsic ellipticity of  $\sim 0.25$  per component (e.g., Hoekstra et al. 2000; Leauthaud et al. 2007), where the exact value depends somewhat on the galaxy type (e.g., van Uitert et al. 2012).

Under the assumption that the original position angles of the galaxies are distributed randomly (see, however, e.g., Hirata & Seljak 2004; Mandelbaum et al. 2006; Schneider & Bridle 2010; Joachimi et al. 2011), the lensing shear can be inferred by averaging over an ensemble of sources. The statistical uncertainty in the measurement of the shear component  $\gamma_i$  is given by

$$\sigma_{\gamma,i} = \sqrt{\frac{\langle \epsilon_i^2 \rangle}{N}} \approx \frac{0.25}{\sqrt{N}}, \quad (23)$$

where  $N$  is the number of galaxies that is averaged to obtain the lensing signal.

If we consider an isolated lens, the effect of weak lensing is a systematic tangential alignment of the images of the background galaxies with respect to the lens. The average tangential distortion, defined as

$$\gamma_T = -(\gamma_1 \cos 2\phi + \gamma_2 \sin 2\phi), \quad (24)$$

can then be used to quantify the lensing signal, where  $\phi$  is the azimuthal angle with respect to the lensing galaxy. This is a convenient quantity, because for *any* mass distribution the azimuthally averaged tangential shear  $\langle \gamma_T \rangle$  as a function of radius from the cluster center can be interpreted as a mass contrast (Miralda-Escude 1991):

$$\langle \gamma_T \rangle(r) = \frac{\bar{\Sigma}(< r) - \bar{\Sigma}(r)}{\Sigma_{\text{crit}}} = \bar{\kappa}(< r) - \bar{\kappa}(r), \quad (25)$$



where  $\bar{\Sigma}(< r)$  is the mean surface density within an aperture of radius  $r$  and  $\bar{\Sigma}(r)$  is the azimuthally averaged surface density at distance  $r$ . In recent years it has become common to present the lensing signal as  $\Delta\Sigma(r) = \Sigma_{\text{crit}}\gamma_T(r)$ , which is convenient when redshifts for the sources and lenses are available (see e.g. Figure 4), as it allows a direct comparison of the amplitude of the lensing signal between samples. Note, however, that the observed signal corresponds to the reduced shear  $g = \gamma/(1 - \kappa)$ . This is not a concern when considering fitting parametric models to the data, as the reduced shear can be computed. Some commonly used examples are discussed below. An important consideration for weak lensing studies, however, is that not all clusters (if any) are well described by simple models.

A simple, but nonetheless useful, model to compare to the data is the singular isothermal sphere (SIS) with  $\rho(r) = \sigma^2/(2\pi Gr^2)$ , where  $\sigma$  is the line-of-sight velocity dispersion. The latter can be compared to results from redshift surveys of cluster members, which provide a dynamical mass estimate. For this mass distribution the tangential shear is given by

$$\gamma_T(r) = \kappa(r) = \frac{r_E}{2r}, \quad (26)$$

where  $r_E$  is the Einstein radius, which can be expressed as

$$r_E = 28''.9 \left( \frac{\sigma}{1000 \text{ km/s}} \right)^2 \beta, \quad (27)$$

where  $\beta \equiv D_{ls}/D_s$  is the ratio of the angular diameter distance between the lens and the source and the angular diameter distance between the observer and the source, which quantifies the dependence of the amplitude of the lensing signal on the source redshift.

For deep ground based observations the number density of sources is  $10 - 20 \text{ arcmin}^{-2}$ , which yields a statistical uncertainty of  $\sim 1''.5$  in the value for the Einstein radius, independent of the cluster mass. The bottom panel of Figure 1 shows an approximate redshift distribution, representative of deep optical observations, with a median redshift  $\sim 0.9$ . For a cluster at intermediate redshift, one finds  $\beta \sim 0.6$  when considering typical ground based observations. This results in a signal-to-noise ratio  $\sim 12$  if  $\sigma = 1000 \text{ km/s}$  (which corresponds to a virial mass of  $M_{\text{vir}} \sim 10^{15} M_{\odot}$ ). Hence, the masses of massive clusters can be determined individually. To study individual lower mass systems ( $\sigma \sim 500 \text{ km/s}$ ) it is necessary to increase the source number density, which can only be done using deep *HST* observations, because the faint galaxies are no longer resolved from the ground.

Similarly, the study of high redshift objects (for which  $\beta$  is smaller) requires space based observations. This is demonstrated in Figure 1 where we plot the average value of  $\beta = \langle D_{ls}/D_s \rangle$  as a function of source redshift for a cluster at  $z = 0.2$  (black curve) and  $z = 0.8$  (red dashed curve). As the amplitude of the lensing signal is proportional to  $\beta$ , it is clear that the signal decreases as a function of lens redshift.

The slope  $\partial\beta/\partial z$  quantifies the sensitivity to the source redshift distribution, which is also larger at high redshifts. This leads to additional noise in the mass measurements unless redshift information for the individual sources is obtained (e.g., Hoekstra et al. 2011b). The importance of good knowledge of the source redshift distribution is discussed further in §3.2.

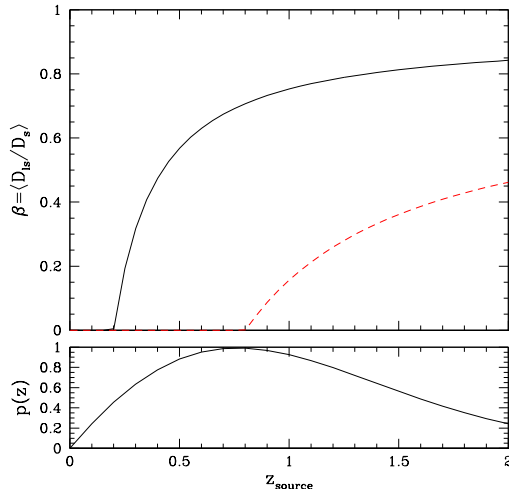


**Fig. 1** The top panel shows the average value of  $\beta = \langle D_{ls}/D_s \rangle$  as a function of source redshift for a cluster at  $z = 0.2$  (black curve) and  $z = 0.8$  (red dashed curve). Note that the asymptotic value is lower for clusters at higher redshifts. The slope of the curve is a measure of the sensitivity to errors or statistical variations in the source redshifts, which is also larger for high redshift clusters. Furthermore, as is indicated by the bottom panel, which shows an approximate redshift distribution representative of deep optical observations, most of the background sources are at redshifts where  $\beta$  rises with a significant slope for the  $z = 0.8$  cluster.

*NFW profile:* Numerical simulations have shown that halos over a wide range in mass can be described by a simple fitting function (Navarro et al. 1997). The density profile is characterized by two parameters, typically the halo mass and the concentration  $c$  (which can be related to a characteristic scale). Observationally, the concentration cannot be constrained well for individual clusters from strong or weak lensing alone. As lensing is sensitive to the total density profile, the contribution from baryons should be included, although their impact should be most prominent in the cluster cores, which are typically not included in the fit. To what extent the profiles are changed depends on the baryon physics (e.g., Duffy et al. 2010), and the current situation is unclear. The uncertainty in the mass estimate is enlarged further by additional structures along the line-of-sight, as discussed in §2.2.1. Instead, it is possible to use the fact that the parameters are found to be correlated in the simulations, albeit with significant scatter. The NFW density profile itself is given by:

$$\rho_{\text{NFW}}(r) = \frac{M_{\text{vir}}}{4\pi f(c)} \frac{1}{r(r+r_s)^2}, \quad (28)$$

where  $M_{\text{vir}}$  is the mass enclosed within the virial radius  $r_{\text{vir}}$ . The concentration parameter  $c$  is defined as the ratio of  $r_{\text{vir}}$  and the scale radius  $r_s$ , and the function  $f(c) = \ln(1+c) - c/(1+c)$ . Analytic expressions for the projected surface density and shear have been derived by Bartelmann (1996) and Wright & Brainerd (2000).

The virial mass is defined with respect to the mean density of the Universe at the redshift of the cluster where the virial overdensity is given by  $\Delta_{\text{vir}} \approx (18\pi^2 +$

$82\xi - 39\xi^2)/\Omega(z)$ , with  $\xi = \Omega(z) - 1$  (Bryan & Norman 1998). For a standard  $\Lambda$ CDM cosmology  $\Delta_{\text{vir}}(z=0) = 337$ . Other definitions are also common in the literature, with overdensities defined with respect to the critical density  $\rho_c$  at the cluster redshift:

$$M_{\Delta} = \frac{4\pi}{3} \Delta \rho_c(z) r_{\Delta}^3, \quad (29)$$

where  $r_{\Delta}$  corresponds to the radius where the mean density is  $\Delta \times \rho_c(z)$ , and  $M_{\Delta}$  is the corresponding enclosed mass. Note that  $M_{200}$  is often referred to as the virial mass. Although similar in value, its definition is in fact different. Given one has to choose a definition of the mass, it is important that this is clearly defined when listing results.

*Aperture mass:* An important advantage of weak lensing is that the shear can be converted into an estimate of the projected mass within an aperture, with relatively few assumptions about the actual mass distribution. For instance the  $\zeta_c$  estimator proposed by Clowe et al. (1998):

$$\zeta_c(r_1) = 2 \int_{r_1}^{r_2} d \ln r \langle \gamma_t \rangle + \frac{2r_{\text{max}}^2}{r_{\text{max}}^2 - r_2^2} \int_{r_2}^{r_{\text{max}}} d \ln r \langle \gamma_t \rangle, \quad (30)$$

can be expressed in terms of the mean dimensionless surface density interior to  $r_1$  relative to the mean surface density in an annulus from  $r_2$  to  $r_{\text{max}}$ :

$$\zeta_c(r_1) = \bar{\kappa}(r' < r_1) - \bar{\kappa}(r_2 < r' < r_{\text{max}}). \quad (31)$$

This result demonstrates that we can determine the surface density within an aperture up to a constant, as was the case for the 2-dimensional reconstruction discussed in §2. Although the surface density in the outer annulus should be small for results based on wide field imaging data, it cannot be ignored. One way to estimate its value, is to use the results from a parametric model that is fit to the data (Hoekstra 2007). This leads to a rather weak model dependence ( $< 10\%$ ) in the estimate of the projected mass.

*Choice of cluster center:* The choice of the cluster center is important when deriving the lensing mass. If the adopted center is offset from the correct value, the contrast is lowered, resulting in a reduction in the observed signal and consequently the lensing mass, as shown in Figure 2. The size of the bias depends on the range in scales used to infer the lensing mass: if the lensing signal at relatively large radii is used, the bias is diminished. Massive clusters typically have well defined central galaxies, whose locations coincide with the peak of the X-ray emission (Bildfell et al. 2008). Note, however, that in merging clusters of galaxies, such as the “Bullet Cluster”, the peak of the X-ray emission may not coincide with the main cluster halos (Clowe et al. 2006a).

The reconstruction of the projected mass distribution (see §4) can in principle be used to select the cluster center. However, even for the most massive clusters, the signal-to-noise ratio is only of order 10, which means that one has to be careful to use the peak position itself, as it will bias the mass estimate high. It is possible to account for this when studying an ensemble of clusters, but it is preferable to use external constraints instead. Weak lensing cluster studies therefore typically adopt the location of the brightest cluster galaxy or the peak in the X-ray emission as the center. The situation is more complicated when considering large samples of clusters, for which high quality X-ray observations may not be available or cannot be obtained because

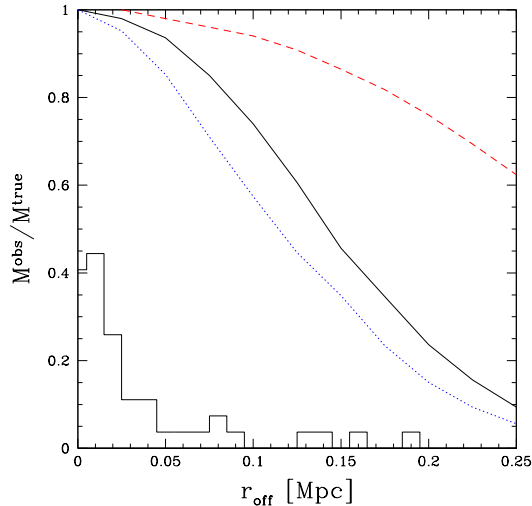


**Fig. 2** From Hoekstra et al. (2011a): plot of the ratio of the inferred lensing mass and true mass as a function of centroid offset  $r_{\text{off}}$ . The lensing mass is obtained by fitting an NFW model to the shear at 200 – 750 kpc (solid black curve) and 0.5 – 1.5 Mpc (dashed red curve). The blue dotted line corresponds to the bias if all data within 750 kpc are used. The distribution of offsets observed for massive clusters by Bildfell et al. (2008) is indicated by the histogram.

the masses of the targets are low. When considering these large samples of clusters the “handpicking” of the center is therefore not practical, nor preferable. Instead the effects of miscentering can be taken into account statistically (Johnston et al. 2007a).

The presence of substructure in the central regions not only complicates the choice of center, but it also leads to biases in the mass estimates when parametric models are fit to the signal. This is because the substructure also lowers the mean density contrast, and thus the shear, compared to a unimodal density distribution (see e.g., Hoekstra et al. 2002a).

### 2.2.1 Cosmic noise

Clusters are integral parts of the cosmic web and are located at the intersections of filaments. Therefore some of this large-scale structure is physically associated with the cluster, which complicates the interpretation of the lensing results, in particular when one wants to compare to other mass indicators (see §6) or determine density profiles (Meneghetti et al. 2012). The correlated large-scale structure has been studied using numerical simulations (e.g. Metzler et al. 2001; Marian et al. 2010; Becker & Kravtsov 2011; Bahé et al. 2012).

As discussed in Becker & Kravtsov (2011) and Rasia et al. (2012), the bias that is introduced depends on how the mass is inferred from the lensing signal. For instance, restricting the model fit to  $\sim R_{200}$  can reduce the bias, compared to fits to the signal at larger radii. Part of this reduction arises from the fact that at large radii the NFW model is not a good description of the signal, for instance due to the presence of substructure and the fact that clusters themselves are clustered. Another approach is

to identify additional structures and fit several halos simultaneously, although Hoekstra et al. (2011b) show that this is of limited use, due to the inherent variation in the density profiles.

For ensemble averaged studies the correlated structure can be accounted for using a halo model approach (e.g. Johnston et al. 2007b; Leauthaud et al. 2010) (also see §2.2.2). The results also depend on whether one adopts a functional form for the relation between the mass and concentration, or whether both are fit simultaneously. This clearly complicates an easy comparison of results, especially when the increasing sample sizes lead to smaller statistical uncertainties. Using numerical simulations Becker & Kravtsov (2011), however, show that the correlated structures are not a major source of uncertainty and that the main source of scatter in scaling relations between lensing mass and other indicators arises from the intrinsic triaxiality of dark matter halos (also see, e.g., Clowe et al. 2004a; Corless & King 2007; Limousin et al. 2012).

Gravitational lensing, however, is sensitive to *all* structure along the line-of-sight, and thus uncorrelated inhomogeneities along a given line-of-sight also contribute to the lensing signal in that direction. The large scale structure (LSS) introduces excess correlations in the shapes of the galaxies, also known as ‘cosmic shear’, which can be used to infer cosmological parameters or study theories of modified gravity (see e.g., Hoekstra & Jain 2008, for a recent review). However, for weak lensing cluster studies this excess variance acts as an additional source of noise, which was first studied by Hoekstra (2001). It arises because we cannot distinguish the cluster signal ( $M_{\text{cl}}$ ) from the LSS contributions ( $M_{\text{LSS}}$ ). Note that the latter contribution vanishes on average, and thus does not bias the mass measurements.

The noise introduced by the large-scale structure can be expressed in terms of the matter power spectrum and a scale dependent filter, similar to what is done for cosmic shear (Hoekstra 2001):

$$\langle M_{\text{LSS}}^2 \rangle(\theta) = 2\pi \int dl P_{\kappa}(l) g(l, \theta)^2, \quad (32)$$

where  $P_{\kappa}(l)$  is the projected convergence power spectrum and the expression for the filter function  $g(l, \theta)$  depends on the adopted statistic. A detailed discussion, including expressions for  $g(l, \theta)$ , can be found in Hoekstra (2001).

Hoekstra (2001) found that the impact of cosmic noise is most important for clusters at low redshift (see the comparison presented in Fig. 3) and if one wants to determine the mass at large radius. This work was extended in Hoekstra (2003) who studied how cosmic noise limits the precision of the determination of mass density profiles from weak lensing. For instance, when an NFW model is fit with mass and concentration as free parameters, the formal uncertainties in both the mass and the concentration can be doubled, compared to the simple statistical uncertainty from the noise of the shapes of the sources. The analytical results obtained in these papers have been confirmed using numerical simulations (Hoekstra et al. 2011b; Becker & Kravtsov 2011).

An interesting question is whether it is possible to reduce or even remove the effects of cosmic noise. Dodelson (2004) proposed a statistical approach which reduces the noise in mass reconstructions, although this might also suppress real structures in individual cases. The main contributors to the cosmic noise signal, however, are clusters and groups of galaxies that can in principle be identified. This was first investigated by de Putter & White (2005) who showed that one would have to include halos down to very low masses ( $< 5 \times 10^{13} M_{\odot}$ ). More importantly the variation in halo profiles and shapes fundamentally limits the precision with which the cosmic noise signal can be

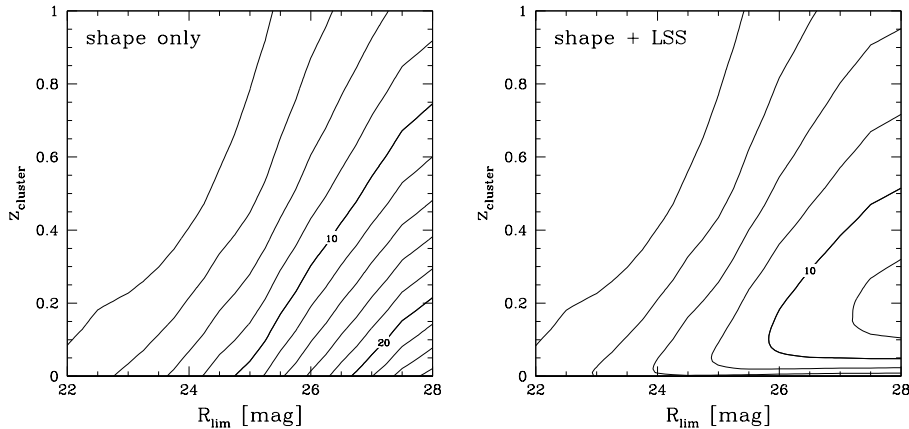


**Fig. 3** Adapted from Hoekstra (2001); *Left panel*: contour plot of the signal-to-noise ratio of a cluster with a SIS density profile and  $\sigma = 1000\text{km/s}$ , as a function of limiting magnitude in the  $R$ -band and cluster redshift, when only the shape noise is considered. *Right panel*: The expected signal-to-noise ratio when the effects of cosmic noise are included. At high redshifts the uncertainty in the weak lensing mass remains dominated by the intrinsic ellipticities of galaxies, but at low redshift cosmic noise becomes an important source of uncertainty.

predicted. This was investigated in more detail in Hoekstra et al. (2011b) who showed that the precision of the mass measurement can be improved only slightly in practice.

A number of studies have now demonstrated that uncorrelated large-scale structure is a significant source of uncertainty for weak lensing mass estimates. It is particularly important for studies that aim to constrain the density profile, as the formal uncertainties on the model parameters are increased substantially. It is therefore important that weak lensing studies of clusters of galaxies take cosmic noise into account.

### 2.2.2 Cluster-mass cross-correlation function

The limited number of background galaxies restricts the study of individual clusters to virial masses that are a few times  $10^{14}M_{\odot}$  or larger. It is, however, possible to study lower mass systems by averaging, or ‘stacking’ their signals: the resulting signal is that of the mass-weighted ensemble. This approach is widely used, and an important application of weak lensing is the study of the properties of dark matter halos around galaxies (e.g. Brainerd et al. 1996; Hoekstra 2004; Mandelbaum et al. 2005; van Uitert et al. 2011). It has also been employed in studies of galaxy groups discovered in the CNOC2 field redshift survey (Hoekstra et al. 2001; Parker et al. 2005) and COSMOS (Leauthaud et al. 2010). In the case of a shallow, but wide survey, stacking the signal around the large number of lenses can be used to compensate for the low number density. This approach has been applied with great success to the SDSS data to measure the ensemble averaged lensing signal around galaxies (e.g., Fischer et al. 2000; Guzik & Seljak 2002; Mandelbaum et al. 2005), groups and clusters (e.g., Mandelbaum et al. 2006; Sheldon et al. 2009).

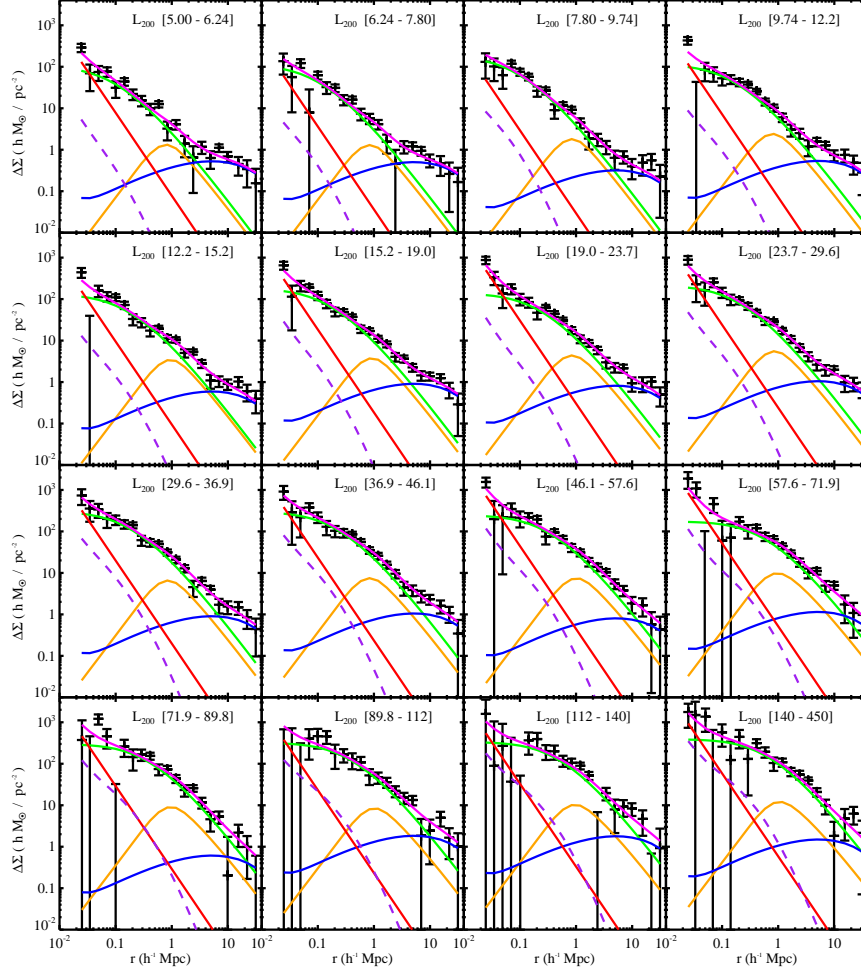


**Fig. 4** Halo model fits to the  $\Delta\Sigma$  profiles of SDSS MaxBCG clusters. For each bin in total  $i$ -band luminosity, a model (magenta) is fitted, consisting of these components: BCG (red), miscentering correction (orange), NFW main halo (green), halo clustering (blue), and non-linear component (purple dashed). Figure from Johnston et al. (2007b).

By dividing the sample of clusters into subsets based on an observable property, such as X-ray luminosity or optical richness, it is possible to determine scaling relations between the observable and the mean mass of the sample (e.g., Johnston et al. 2007b; Rykoff et al. 2008; Leauthaud et al. 2010). It is important to note here that the interpretation of the result requires knowledge of the intrinsic scatter between the mass and the quantity of interest. Only for high masses the latter can be determined observationally. For low masses one relies on numerical simulations to provide guidance.

Figure 4 shows the lensing signal as a function of luminosity  $L_{200}$  around clusters from the SDSS MaxBCG sample (Koester et al. 2007), which contains 13,823  $0.1 < z < 0.3$  clusters identified in 7500  $\text{deg}^2$  of SDSS data. The lensing signal was measured by Sheldon et al. (2009) using a source catalogue of  $2.8 \times 10^6$  galaxies for which SDSS lensing-quality data and photometric redshifts are available. A clear lensing signal is detected in all luminosity bins.

The ensemble averaged signal corresponds to the cluster-mass cross-correlation function. This reflects that only on small scales the signal arising from the main cluster halo dominates, whereas at large radii it is sensitive to the clustering of clusters, which in fact provides additional information. It is possible to compute the combined signal using a (semi-)analytical approach suggested by Seljak (2000): the halo-model. It uses the fact that individual dark matter halos are well described by the NFW profile, and that we can compute the halo mass function and the clustering of halos for a given cosmology. Much ongoing work focusses on ways to improve the shortcomings of the halo-model.

Here we briefly review the main components of the model that are used to model the lensing signal around clusters of galaxies (see e.g. Johnston et al. 2007b, for more details). On small scales the lensing signal is computed from the NFW model, which is convolved with a probability density distribution of offsets from the adopted center. As discussed in §2.2 this can be determined fairly directly for massive clusters, but for large samples of (optically selected) clusters a distribution of offsets needs to be adopted, for instance based on numerical simulations. This first contribution describes the cluster dark matter halo (and implicitly assumes that the ICM follows a similar distribution; see Semboloni et al. (2011) for a study where this assumption is relaxed). The signal of the BCG is also added, and can be approximated by a point mass.

On large scales the fact that clusters themselves are part of the cosmic web and thus are clustered causes an additional signal. This can be seen clearly in Figure 4 for the lower mass clusters (top-left corner): the lensing signal shows a clear excess compared to the NFW signal (green curve). The signal from these neighbouring halos is described by the two-halo term (Seljak 2000) and is indicated by the blue curves. This term requires the calculation of the correlation function in linear perturbation theory and a prescription for the linear bias as a function of mass and redshift. Comparison of the predicted amplitude to the observed value can be used to test models of structure formation or to constrain the normalisation of the matter power spectrum (see §5.3 in Johnston et al. 2007b).

### 2.2.3 Magnification

The measurement of the magnification of galaxies provides a complementary way to study the mass distribution. Especially in the case of observations in multiple filters, the data used for the shear analysis allow for a magnification measurement as well. The actual magnification cannot be measured for a single object because the intrinsic flux is typically unknown. Instead, the signal can be inferred from the change in the source number counts. Such a change arises from the balance between two competing effects. On the one hand the actual volume that is surveyed is reduced, because the solid angle behind the cluster is enlarged. However, the fluxes of the sources in this smaller volume are boosted, thus increasing the limiting magnitude. As a consequence, the net change in source surface density depends not only on the mass of the lens, but also on the steepness of the intrinsic luminosity function of the sources. If it is steep, the increase



in limiting magnitude wins over the reduction in solid angle, and an excess of sources is observed. If the number counts instead are shallow, a reduction in the source number density is observed.

A correct interpretation of the result only requires accurate photometry and knowledge of the (unlensed) luminosity function. Therefore the requirements on the PSF are much less stringent compared to the shear-based approach. The main systematics in this case are the uniformity of the photometry and completeness of the source sample (to establish the slope of the luminosity function). However, contamination of the source population by cluster members needs to be avoided as well. This is a larger issue for magnification studies, compared to measurements using shear. As discussed in Hildebrandt et al. (2009) Lyman Break Galaxies (LBGs) can provide such a clean sample of high redshift sources, although their number density is relatively low.

The uncertainty in the measurement of magnification is determined by variations in the number density (i.e., a combination of Poisson noise and the clustering of the sources). As a result, the signal-to-noise ratio per source galaxy is typically lower, compared to a shear measurement. It is difficult to measure reliable shapes for distant sources using typical ground based data, because they cannot be resolved. Their magnitudes, however, can still be measured, and thus also the magnification signal. Hence, the signal-to-noise of the magnification signal can be higher than the shear signal in the case of high redshift objects. The low number density of LBGs prevents precise measurements for individual systems, but it has recently been used to constrain masses of a sample of  $z \sim 1$  clusters by Hildebrandt et al. (2011) for the first time using this approach. The same technique was used by Ford et al. (2012) to study galaxy groups.

If photometric redshifts are available, it should be possible to increase the number density of sources that can be used, although the performance of photometric redshift codes in the presence of a large number of cluster members needs to be investigated in detail. Another approach is to consider the number density of galaxies redder than the cluster red-sequence as proposed by Broadhurst et al. (1995). This may be better suited for ensembles of clusters as well, as the stronger clustering of red galaxies increases the noise in the measurement. For a sample of massive clusters Umetsu et al. (2011) obtained good agreement between the magnification signal and that inferred from the shear analysis.

Schmidt et al. (2012) used *HST* imaging of the COSMOS field to measure the magnification signal by combining the magnitudes (and redshifts) with estimates of the sizes of the source galaxies. The signal-to-noise ratio is 40% of what is achieved from shear measurement. Although this approach requires excellent imaging quality data, it comes at no additional cost. Finally Bauer et al. (2012) used a sample of variable quasars from the SDSS. In this case the magnification signal is determined by comparing the luminosity to the one expected based on the correlation between the amplitude of variability and the intrinsic luminosity. These recent results highlight the growing interest in using magnification as an additional way to determine cluster masses.

### 3 Measuring the weak lensing signal

Having introduced the observables and discussed how these can be used to map the matter distribution and determine cluster masses, we now turn to the practical aspects of the measurements. Although cluster lensing studies share many common issues with

other applications, such as galaxy-galaxy lensing and cosmic shear, there are also a number of issues that are particularly important for cluster lensing.

Starting with the measurement of the galaxy shapes, discussed in more detail in §3.1, the shear in the inner regions of clusters can be substantial, to a level where the biases in the shape measurement algorithms are not (yet) well understood. However, even a perfect measurement of the shapes of galaxies does not imply an unbiased mass estimate. This is because the interpretation of the lensing signal requires estimates for the level of contamination by cluster members and knowledge of the source redshift distribution, both of which are detailed in §3.2.

### 3.1 Shape measurements

The alignment in the shapes of the sources induced by weak lensing is subtle and is often dwarfed by the anisotropy of the PSF, which introduces an additive bias. The PSF also circularizes the images, leading to a reduction of the amplitude of the lensing signal, i.e. a multiplicative bias. Although this bias can be reduced using space based observations, the PSF circularization can never be ignored. The resulting images are sampled onto the pixels of the detector, which itself can introduce problems: charge transfer inefficiency is an important systematic in space based observations, where the background is low (see Massey et al. 2012, for a detailed discussion of how the various systematic biases affect weak lensing studies). Finally the images of the faint galaxies that carry most of the signal are noisy, which complicates matter further (e.g., Melchior & Viola 2012; Refregier et al. 2012).

These effects need to be corrected for if we want to determine accurate cluster masses from weak gravitational lensing. This not only requires an algorithm that can undo the bias caused by the PSF, but also an accurate model for the PSF itself (Hoekstra 2004). The model is typically determined from a sample of moderately bright stars that are identified in the actual data. Depending on the correction scheme, the images of these stars are either modeled or shape parameters are determined. To describe the spatial variation of the PSF the model is interpolated, typically using a low order polynomial function of the coordinates. Much of the recent cluster studies use data from cameras that cover the focal plane with a mosaic of detectors. The gaps between the detectors are filled by dithering the observations. This can lead to additional structure in the PSF, where the impact depends on the observing strategy. Alternatively, one can homogenize the PSF before the images are combined, which can also improve the fidelity of photometric redshift measurements (Hildebrandt et al. 2012). Another approach is to develop techniques that can operate on unstacked images (Miller et al. 2012).

Fortunately, in comparison to cosmic shear studies, the uncertainties in the PSF model are not an important source of systematic when determining cluster masses. This is because the mass estimate involves integrating over the tangential shear as a function of radius, and local deviations are suppressed in the averaging. Consequently the cluster mass measurements are also relatively insensitive to limitations of the algorithms to correct for PSF anisotropy, although the latter can be important when considering mass reconstructions.

Once the spatial variation of the PSF has been modelled, the next step is to measure the galaxy shapes and correct them for the various observational distortions. This is the most critical part of the analysis, and improving the correction algorithms continues to

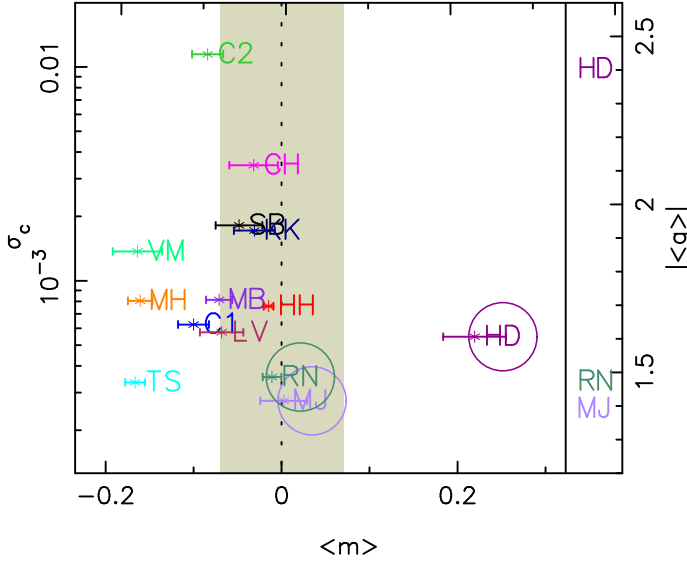


**Fig. 5** Measurement of the calibration bias  $m$  and PSF residuals  $\sigma_c$  from Heymans et al. (2006). The ideal method has  $m = 0$  and small  $\sigma_c$ . The shaded region indicates a bias of less than 7%. Methods that were used for published cosmic shear results were found to have biases of the order of a few percent. We refer the reader to Heymans et al. (2006) for a detailed description of the symbols and methodology.

be an active area of research. It is therefore not surprising that a range of algorithms has been developed to tackle this problem. An overview of a number of these can be found in Heymans et al. (2006), Massey et al. (2007), Bridle et al. (2010) and Kitching et al. (2012).

Shape measurement methods can be roughly separated into two classes. One approach is to measure the weighted moments of the images, and correct these analytically for the effects of the PSF. The KSB algorithm proposed by Kaiser et al. (1995) falls into this category (for modifications to the original algorithm see Luppino & Kaiser 1997; Hoekstra et al. 1998). Despite a number of shortcomings, it remains one of the most widely used methods. A nice feature is that the corrections for PSF anisotropy and circularization are separate operations. The algorithm is, however, limited by the assumptions made about the PSF and galaxy profiles.

A key assumption in the derivation is that the PSF can be described as a convolution of a compact anisotropic kernel and a large isotropic kernel. This may be a reasonable approximation for ground-based data, but it is less so for diffraction-limited observations from space. An open question is whether this can be circumvented by PSF homogenisation with a kernel that ensures that the resulting PSF is Gaussian (Kuijken 2008). More general algorithms have also been proposed by Melchior et al. (2011) and Bernstein (2010), and work is continuing to improve the algorithms.

The other class of methods attempts to fit the observed images with sufficiently versatile models. The basis functions are often chosen such that the (de)convolution can be performed analytically. For instance Kuijken (1999) explored the possibility of modeling galaxies as sums of Gaussians. Another basis set was proposed by Refregier

& Bacon (2003). This shapelet expansion has proven useful to model the PSF of real data (Kuijken 2008; Hildebrandt et al. 2012), but has not been used widely for actual lensing measurements. Finally we mention lensfit (Miller et al. 2007, 2012), which is a Bayesian algorithm that fits galaxies with a bulge+disk model and has been used recently to analyse data from the CFHT Legacy Survey (Heymans et al. 2012).

*Testing algorithm performance:* An important advantage of weak lensing is that the algorithms can be tested using realistic simulations of the actual data (see e.g., Hoekstra et al. 1998; Erben et al. 2001; Hoekstra et al. 2002b, for early tests). To compare how well methods perform, it is convenient to consider the bias in the shape measurement as the combination of a multiplicative bias  $m$  and an additive bias  $c$

$$\gamma_{\text{obs}} = (1 + m)\gamma_{\text{true}} + c. \quad (33)$$

This parametrization was used by the Shear TEsting Programme (STEP; Heymans et al. 2006), which was the first collaborative effort of the weak lensing community to test the performance of the various algorithms. The first study presented in Heymans et al. (2006) involved the blind analysis of simulated galaxies with relatively simple morphologies. In Massey et al. (2007) more complicated galaxies were examined. The results of Heymans et al. (2006) are reproduced in Figure 5. These studies showed that the dominant source of bias is the correction for the size of the PSF, quantified by  $m$ , although the most successful methods were able to achieve 1 – 2% accuracy.

Such biases may seem small, but the limitations become dominant for cluster samples that exceed  $\sim 100$  massive clusters. We also note that these studies did not test the high shear regime. However, in the case of aperture masses or when the model fits are restricted to larger radii, this is not a serious problem.

Heymans et al. (2006) and Massey et al. (2007) provided an important benchmark for the performance of ground-based weak lensing studies, but also clearly indicated that further progress is needed. For instance biases as a function of object size and magnitude (or signal-to-noise ratio) have been identified. To stimulate new ideas to solve the problem of shape measurement for future projects, the Gravitational LEnsing Accuracy Testing 2008 (GREAT08) Challenge (Bridle et al. 2010) aimed to involve researchers outside the traditional weak lensing community. This early challenge was followed by GREAT10, which improved the comparison methodology. The results presented in Kitching et al. (2012) showed a factor of 3 improvement compared to the earlier studies, with the best methods now achieving sub-percent biases on average. Further progress is expected in coming years, in preparation for ambitious dark energy projects such as *Euclid*<sup>1</sup> (Laureijs et al. 2011).

### 3.2 The importance of redshift information

To relate the lensing signal to physical quantities, such as the mass, we need to determine the value for the critical surface density  $\Sigma_{\text{crit}}$  (Eqn. 6), which requires knowledge of the redshifts of the faint source galaxies. Furthermore, the sample of galaxies used to compute the lensing signal may contain cluster members which dilute the signal. In this section we review these two important issues.

---

<sup>1</sup> <http://www.euclid-ec.org>

### 3.2.1 Source redshifts

The faintest galaxies that are suitable for weak gravitational lensing measurements are typically much fainter than galaxies targeted efficiently in spectroscopic redshift measurements. Even if some redshifts could be obtained, the resulting sample would be highly incomplete at the magnitudes of interest. Hence, it is generally unfeasible (because of the enormous cost in telescope time) to determine the redshifts of a significant fraction of the weakly lensed sources.

Fortunately, the redshifts do not need to be determined with high precision, and photometric redshift estimates are sufficient. As discussed in §2.2 and shown in Figure 1, for a cluster at a known distance  $D_l$ , the relevant quantity is  $\beta \equiv D_{ls}/D_s$ : the derived lens mass will scale linearly with  $\beta$ , and any systematic error in the determination of this parameter will translate directly into a corresponding bias in the mass. Note that the inclusion of unlensed foreground galaxies is not a problem *per se* as long as the foreground contribution in the source galaxy catalogue can be modeled and included in the estimate of  $\langle\beta\rangle = \langle\max(0, D_{ls}/D_s)\rangle$ .

Typically, the value of  $\beta$  is determined by relating the source galaxy catalogues to photometric redshift catalogues in the literature, e.g. from the COSMOS survey (Ilbert et al. 2009) or the Hubble Ultra Deep Field (Coe et al. 2006) or the CFHTLS Deep fields (Ilbert et al. 2006), while taking into account the weights assigned to the background galaxies of different magnitudes when making the weak shear measurement. Hence it is not necessary to determine photometric redshifts of the galaxies in the actual cluster observations, although the benefits of such ancillary information are discussed below. In cases where the imaging data for the lensing measurements go even deeper than the photometric redshift data sets, extrapolation will be required, typically using a parametrization of the galaxy redshift distribution as a function of magnitude (see e.g., Schrabback et al. 2010). As such galaxies are often at high redshifts, the lack of deep near-IR data provides another challenge, although the situation keeps improving.

The required accuracy is naturally determined by the scientific goals of a cluster study. If the goal is to determine lensing masses for a small number of individual clusters, it is typically sufficient to determine an effective mean value of  $\beta$ . Generally the source galaxy population will follow a broad distribution in redshift. However, it is possible to define an effective source galaxy redshift such that  $D_{ls}/D_s(z_{\text{eff}}) = \langle\beta\rangle$  and proceed as if all background galaxies are located at this redshift. Note that it is important to correct this value for the contamination by cluster galaxies (see §3.2.2). For statistical studies based on larger samples of clusters (e.g., scaling relations), care must be taken to avoid systematic effects caused by inadequate redshift information for the source galaxy population.

The effective source redshift can be used for low redshift clusters ( $z < 0.3$ ), where the estimate for  $\beta$  is robust and systematic errors are negligible compared to the statistical errors. For high redshift clusters ( $z > 0.6$ ) the slope  $\partial\beta/\partial z$  is steeper (see Figure 1), which implies a larger sensitivity to systematic errors in the source redshifts, but also a larger sensitivity to the width of the redshift distribution. As discussed by Seitz & Schneider (1997) and Hoekstra et al. (2000) this will introduce an overestimate of the shear of order

$$1 + \left[ \frac{\langle\beta^2\rangle}{\langle\beta\rangle^2} - 1 \right] \kappa. \quad (34)$$

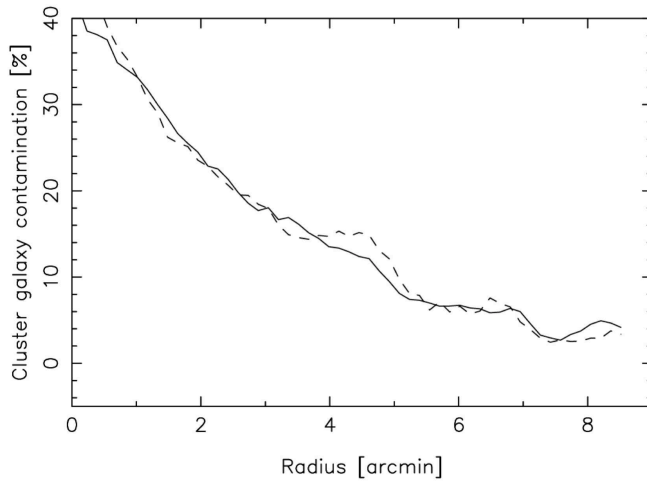


**Fig. 6** Illustration of typical observed levels of cluster galaxy contamination in faint galaxy catalogs as a function of distance from the cluster center. The solid line represents an average of six X-ray luminous ( $L_{X,0.1-2.4\text{keV}} \geq 6 \times 10^{44} \text{ erg s}^{-1}$ ) clusters at an average redshift  $\langle z \rangle = 0.31$ , while the dashed line represents an average of five similarly X-ray luminous clusters at  $\langle z \rangle = 0.23$ . Figure taken from Pedersen & Dahle (2007).

This systematic error will be small for clusters at low redshift and is frequently ignored in the literature, but it can be relevant for clusters at high redshift, in particular for lensing-based studies of matter density profiles which use measurements at radii where the convergence  $\kappa$  is not  $\ll 1$ .

Although it is possible to interpret the results of large samples of clusters with an average redshift distribution, the actual redshift distribution of sources will vary. At large radii, where the signal is averaged over many galaxies on relatively large scales, the source redshift distribution is expected to be close to the average. At small radii this is not a good representation, because the small number of sources samples the average distribution only sparsely. This leads to additional noise if photometric redshifts for the sources are not available. At low redshift where variations in the redshift distribution lead to only small variations in  $\langle \beta \rangle$ , this is still a minor source of error. This is no longer the case at high redshift, where the number density of background galaxies is low and  $\langle \beta \rangle$  depends strongly on the actual redshift distribution.

This was studied in Hoekstra et al. (2011b) who showed that the lack of redshift information for the individual sources leads to an additional uncertainty in the shear estimate on scales  $< 4'$ . As expected, the scatter increases with redshift and becomes a relevant source of noise for high redshift clusters  $z > 0.6$ . Hence, studies of high redshift clusters benefit greatly from photometric redshifts for the sources. This not only reduces the noise due to variations from the average redshift distribution, but also boosts the signal by removing foreground (and cluster) galaxies.

### 3.2.2 Contamination by cluster galaxies

Without redshift information for individual galaxies, one encounters the problem of contamination by (unlensed) cluster galaxies which will dilute the observed shear signal

and cause an underestimate of the cluster mass. Since the faint galaxies are clustered (though not necessarily with the same radial distribution as their brighter counterparts), the amount of such dilution will be a function of radius. As shown in Figure 6 the level of contamination ranges from tens of percent in the innermost parts of the cluster, while it is essentially negligible at large radii. If left unaccounted for, the resulting reduction in the lensing signal at small radii may be misinterpreted as a flattening of the density profile. Hence a careful treatment of the contamination by cluster members is particularly important when studying the density profiles of clusters using weak lensing (see §5.1).

The reliability of the separation of background and cluster galaxies generally increases with the number of passbands available, with full photometric redshift information for the sources performing best. However, the limited availability of telescope time at major observatories generally dictates the use of a minimum set of filters sufficient to limit the bias caused by cluster galaxy contamination to an acceptable level. In this section we discuss possible approaches in increasing order of accuracy (and therefore cost).

*Statistical correction based on galaxy overdensity as a function of radius:* State-of-the-art wide-field mosaic CCD cameras allow us to efficiently image well beyond the virial radius of all but the most nearby clusters. The galaxy number density measured in the outskirts of the observed field can then be taken as the background level, assumed to be unaffected by the cluster. A radial correction for the cluster galaxy contamination can be derived from the measured excess of counts at smaller radii (see Figure 6).

This correction becomes unreliable in the innermost regions where the observed background galaxy number density can be affected by magnification (see §2.2.3), or substructure in the cluster core. In addition, there will be large statistical uncertainties because of the low numbers of galaxies. This approach can be used to estimate cluster masses (Pedersen & Dahle 2007; Hoekstra 2007), provided the small scale lensing signal is avoided. We note, however, that this correction is less suitable for studies of cluster density profiles, which require reliable weak lensing measurements over a wide range of radii.

*Exclusion of cluster galaxies in a color-magnitude diagram:* The early-type cluster galaxies form a tight sequence in a color-magnitude diagram, which can easily be recognized for massive, low- $z$  clusters. For the color indices of most typical combinations of two broadband optical filters, and for K-corrections given by the spectral energy distributions of normal galaxies, the red sequence galaxies will be redder than any other galaxies in the cluster or at lower redshifts. Hence, by only picking galaxies redder than, and clearly separated from, the red sequence, a robust selection of background galaxies with negligible contamination can be performed (e.g., Okabe et al. 2010).

The robustness of a red background galaxy selection comes at a considerable prize in terms of signal-to-noise, since most lensed background galaxies are bluer than the red sequence and will be omitted by this method. While such a selection is still feasible using e.g., deep  $V$  and  $i'$ -band data for a low-redshift ( $z = 0.18$ ) cluster such as Abell 1689 (Broadhurst et al. 2005), the number of red background galaxies decreases rapidly with increasing cluster redshift (because the red-sequence shifts to redder colors).

The number of source galaxies can be substantially increased by avoiding the red-sequence, but including galaxies that are sufficiently bluer. Such a selection will inevitably include some residual contamination from actively star-forming blue dwarf

galaxies in the cluster, which may have a significantly shallower radial distribution than their brighter, redder counterparts (e.g., Pracy et al. 2004, find a slope  $\alpha = 0.63$  for the radial distribution of the “intermediate” dwarf population  $-18 < R_{F606W} < -15$  in Abell 2218). This residual contamination may be estimated and removed using the methods outlined above, based on galaxy overdensity as a function of radius (e.g., Hoekstra 2007).

*Exclusion of cluster galaxies in a color-color diagram:* Adding observations in a third passband enables a refined exclusion of cluster galaxies based on their position in the color-color space represented by the three filters. By convolving template spectral energy distributions derived empirically and/or from galaxy evolution models with the bandpasses of the filters, the locations of different types of galaxies in color-color space as a function of redshift may be identified. This was used by Medezinski et al. (2010) to study the cluster light distribution and to minimize contamination of the sample of source galaxies.

Thus, regions of color-color space where galaxies at redshifts lower than, or similar to, the cluster may reside can be excluded from further analysis. This provides a robust method to exclude foreground and cluster galaxies which may also be checked against photometric redshift catalogues. Recently, High et al. (2012) applied this approach using *gri* observations of clusters with  $0.28 < z < 0.43$ . The resulting source sample did not show appreciable clustering, suggesting that this selection works well for intermediate redshift clusters. Umetsu et al. (2012) present results for their study of MACS J1206.2-0847, a massive  $z = 0.439$  cluster. For the blue sources they find a constant number density with radius, but the red source counts decline towards the center, a consequence of magnification. Finally, Applegate et al. (2012) compared the performance of such color-cuts to the case where photometric redshift information is available.

*Photometric redshifts:* Having redshift information for individual sources naturally provides the best separation of sources and cluster galaxies. Although targeted weak lensing studies have limited the number of filters, focusing instead on larger numbers of clusters, the next generation cosmic shear studies will observe large areas of the sky in multiple filters, providing large samples of clusters *and* sources with redshifts. For instance, Wittman et al. (2003) provide an example of a massive galaxy cluster at  $z = 0.68$  discovered in the Deep Lens Survey data.

The Cluster Lensing And Supernova survey with Hubble (CLASH; Postman et al. 2012) will target 25 clusters and provide *HST* photometry in 16 filters. This will provide excellent photometric redshift information for the sources, and will enable them to examine the redshift dependence of the lensing signal in unprecedented detail, which can be used to constrain cosmological parameters (e.g., Golse et al. 2002; Jain & Taylor 2003). The first results have been published recently, based on strong lensing of multiple sources with known redshifts behind the cluster (Jullo et al. 2010) and by weak lensing measurements of a stack of lower-mass galaxy groups (Taylor et al. 2012). Given the small differences predicted for different cosmological models, it is presently unclear how powerful this technique may prove to be. Any deviations between the assumed and actual cluster mass distribution would introduce biases which might be difficult to disentangle from the cosmological signal (Zieser & Bartelmann 2012).

The amplitude of the lensing signal as a function of source redshift can also be used to gain information about the 3D distribution of the density field. This “tomographic”



approach has been used to map the mass density field towards the A901/2 supercluster (Taylor et al. 2004; Simon et al. 2012). While such data can be used to simultaneously derive redshifts and masses directly for structures along the line of sight, well-defined structures such as rich galaxy clusters would in any case be readily identifiable from the photometric data alone, and the derived cluster redshifts from weak lensing tomography would have much larger uncertainties (typically  $\Delta z \sim 0.2$  or larger) than any photometric redshifts that could be derived from the same data set. Hence, the utility of this technique is more as a powerful method of statistically probing structure growth as a function of redshift based on large data sets for cosmic shear measurements, rather than as an efficient method for finding large samples of galaxy clusters.

## 4 Mass reconstruction

In §2.2 we already discussed that it is possible to reconstruct the projected matter distribution from the observed shear field. Unfortunately Eqn. 12, derived by Kaiser & Squires (1993), is not very practical, as its evaluation requires data out to infinity. Furthermore a smoothing of the results/data is required because the shear is only sampled at the locations of the source galaxies. Finally, the reconstruction assumes that we have measured the shear, which can deviate appreciably from the observed reduced shear in the central regions of clusters. The latter problem can, however, be solved by iteration (Seitz & Schneider 1995).

The use of Eqn 12 leads to biased results if data for a relatively small area are available (small in comparison to the extent of the cluster). This was a serious issue for early ground-based studies, carried out in the '90s, before wide-field imagers became available. To solve this problem a number of finite-field inversion techniques were developed (e.g. Seitz & Schneider 1995; Squires & Kaiser 1996; Seitz & Schneider 1996, 2001). Another approach is the use of maximum-likelihood methods, which avoid this problem altogether (e.g. Bartelmann et al. 1996; Seitz et al. 1998). Modern weak lensing studies of clusters employ wide field imagers, which alleviates the issue by having observations over a finite area of the sky. It can, however, still be a relevant problem for *HST* observations of galaxy clusters, which cover only a small area.

### 4.1 Combination of Strong and Weak Lensing Data

Strong and weak lensing observations of a cluster lens naturally probe complementary regimes, as strong lensing information can accurately constrain the matter distribution in the cluster center whereas weak lensing traces mass out to the cluster outskirts. The idea of combining both lensing methods into a single lensing mass profile is hence straightforward, in particular as a means of breaking the mass-sheet-degeneracy. In practice, however, combined strong and weak lensing mass reconstructions continue to be technically challenging.

Since the first developments of algorithms to combine strong and weak lensing information (Abdelsalam et al. 1998; Bartelmann et al. 1996; Seitz et al. 1998), combined lensing methods have been applied to a small number of clusters. Current methods include the algorithms discussed in Bradač et al. (2005), Cacciato et al. (2006), Diego et al. (2007) and Merten et al. (2009). One of the most important results, based in

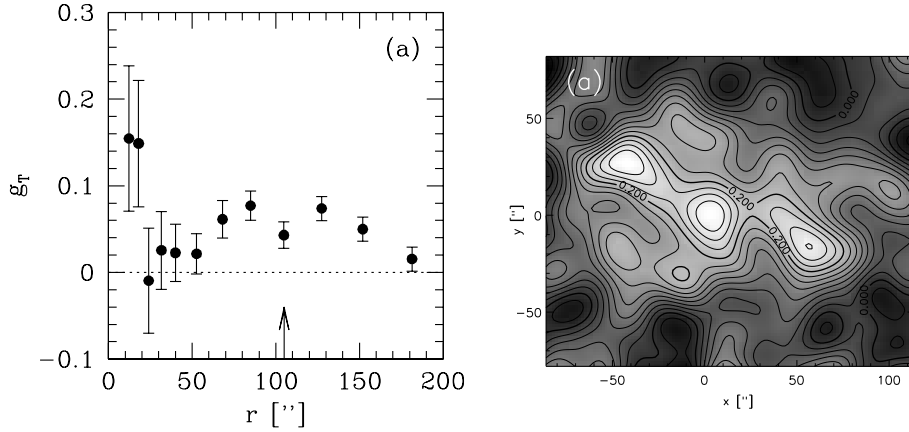


**Fig. 7** Figures from the weak lensing study of the  $z = 0.83$  cluster MS1054-03 by Hoekstra et al. (2000). The left panel shows the azimuthally averaged tangential distortion as a function of distance to the cluster center. Note that the signal drops to zero at  $r \sim 30''$ , before rising again, which reflects the fact that the cluster consists of multiple clumps, which is evident from the mass reconstruction shown in the right panel. The mass distribution in the central regions of this massive high redshift cluster is not well described by a simple parametric model.

part on a joint strong and weak lensing reconstruction, is the discovery of the dissociation between the dark matter distribution and the ICM in the “Bullet cluster” 1ES 0657–558 (Bradač et al. 2006, also see below). Combining information from both regimes is relatively straightforward when considering parametric methods, such as the one developed by Jullo et al. (2007), which as used by Limousin et al. (2010) to study the massive  $z = 0.545$  cluster MACS J1423.8+2404.

These state-of-the-art joint strong and weak lensing algorithms are based on optimising a suitable function  $\chi^2[\Psi(\mathbf{x})] = \chi_{\text{SL}}^2[\Psi(\mathbf{x})] + \chi_{\text{WL}}^2[\Psi(\mathbf{x})] + R[\Psi(\mathbf{x})]$  with the deflection potential  $\Psi(\mathbf{x})$  in every cell of a grid as a free parameter. The minimisation problem can in general only be solved iteratively and a regularisation term  $R[\Psi(\mathbf{x})]$  is needed to ensure numerical stability and smoothness of the resulting deflection potential. Complexity arises due to the different nature of strong lensing and weak lensing constraints, reflected in the respective  $\chi^2$ -functions, notably in the error estimation. Strong lensing gives a small number (in terms of degrees of freedom) of highly significant constraints, localised in a small area within the cluster’s Einstein radius. These have to be calibrated well against the much larger number of weak lensing galaxies which are distributed over a large field-of-view. These issues can be addressed by using a grid of adaptive mesh size, giving special care to finite differencing interpolation.

#### 4.2 Results from Mass Reconstruction

Non-parametric mass reconstructions are not particularly useful for cluster mass determinations, because the observed shear field needs to be smoothed to suppress noise in the mass map (especially when considering mass estimates on small scales). Hence, mass measurements are best carried out using parametric model fits to the data, or

using aperture mass statistics, as discussed in §2.2. However, as many clusters are complex, especially at high redshifts where they are still being formed, parametric model fits may not always be appropriate. This is highlighted in Figure 7. The left panel shows the lensing signal as a function of radius for the massive  $z = 0.83$  cluster of galaxies MS1054-03, studied using deep *HST* observations by Hoekstra et al. (2000). The amplitude of the signal does not decrease monotonically, and the mass reconstruction, shown in the right panel, reveals the reason for this: the cluster consists of three distinct clumps. The ability to identify significant substructures is an important application of (non-parametric) cluster mass reconstructions.

Hence, mass reconstructions of galaxy clusters can play an important role in determining whether a cluster can be considered as a “relaxed” or a possibly “merging” system. Complex structure in the mass map is, however, not necessarily related to merging activity, as lensing probes the projected mass distribution. For instance, Israel et al. (2012) have presented a case of a  $z = 0.45$  cluster, likely seen through a filament at  $z = 0.22$ , connecting several structures to a massive foreground cluster. This mass distribution results in an extended shear plateau and complicates the mass determination of the more distant cluster. Using information from the mass map in conjunction with other probes, in particular X-rays, it is possible to account for such cases and retain them in the analysis of a pre-defined X-ray sample. Another example was presented in Israel et al. (2010), although in this case the foreground concentration of galaxies does not seem to impede the weak lensing mass measurement. Studying cluster maps thus helps the interpretation of anomalous results in profile fits to cluster shear signals in the context of cosmology from increasingly large and distant cluster samples.

However, arguably the most interesting class of objects for detailed mass reconstruction studies are merging clusters. Obviously, the description of the mass distribution by a smooth, highly symmetric mass profile, such as Eqn. 28, breaks down. This is particularly true in the case of a major merger. In these cases the so-called “non-parametric” methods are clearly favoured. What makes mass reconstructions of merging clusters so important is the possibility that during certain phases of a merger the “collision-less” dark matter and galaxy components can segregate from the more dissipative ICM. Given a favourable alignment with respect to the line-of-sight, this can lead to a measurable offset between the lensing and X-ray surface brightness peaks. Over the last years, a small number of such “dissociative mergers” (Dawson et al. 2011) has been discovered and subsequently studied using a range of methods and instruments. The defining feature of a dissociative merger is the offset between the ICM and total mass peaks (as inferred by weak lensing).

The prototype of such systems is the “Bullet cluster” 1ES 0657–558. This system, an advanced stage of a merger in which an infalling cluster has already passed through the core of the more massive component almost in the plane of the sky, was the first in which a significant separation between the X-ray and weak lensing mass peaks of both subclusters was discovered (Clowe et al. 2004b; Markevitch et al. 2004). Using a finite field inversion method and *HST* data, Clowe et al. (2006b) determined the separation to be significant at the  $8\sigma$  level, which was confirmed in an analysis also incorporating strong lensing data (Bradač et al. 2006). The interpretation, also corroborated by follow-up studies (e.g. Springel & Farrar 2007), is that while the ICM of the two clusters experienced deceleration due to the collision (as indicated best by the shock visible with *Chandra*), the dark matter halos passed through each other without significant interaction. An upper bound on the self-interaction cross-section of dark matter particles can be inferred from the displacement between the Dark Matter and

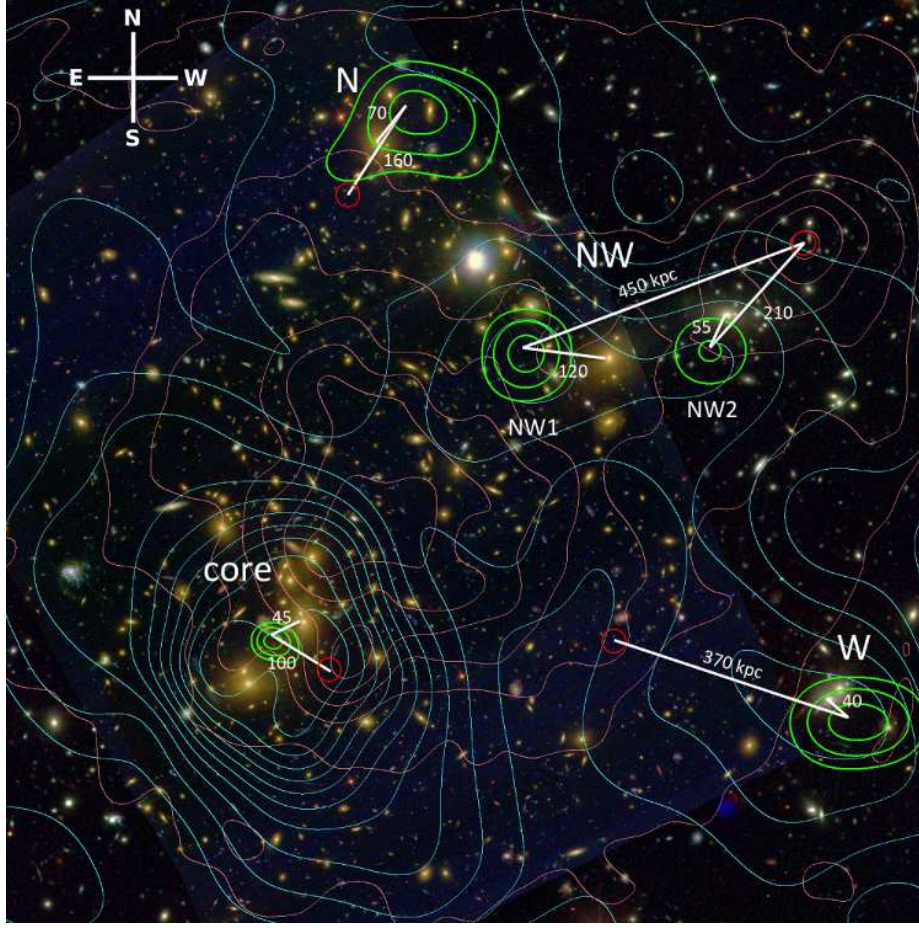


**Fig. 8** Mass reconstruction of Abell 2744 (“Pandora’s cluster”), overlaid on a  $4' \times 4'$  *HST*/VLT/Subaru false-color mosaic: The reconstructed surface mass density is indicated by the cyan contours, while X-ray surface brightness contours are given in magenta. Green contours show mass peaks from bootstrap resampling. Contour levels are chosen at 86%, 61%, and 37 % of the respective maximum peak likelihood. Relevant distances to bright galaxies and local gas peaks are highlighted by rulers. Figure from Merten et al. (2011).

gas peaks. Markevitch et al. (2004) constrain the cross-section to  $< 1 \text{ cm}^2 \text{ g}^{-1}$ , resulting in the most direct piece of evidence for the existence of non-baryonic dark matter to date<sup>2</sup>.

Another interesting system is Abell 2744, where at least four different subclumps each with masses  $> 10^{14} M_{\odot}$ , were discovered by applying the Merten et al. (2009) technique to a combination of strong and weak lensing data collected using the *Hubble Space Telescope*, VLT, and Subaru telescopes. Using these data, as well as deep *Chandra*

<sup>2</sup> Even tighter constraints on the collision cross-section were derived by Meneghetti et al. (2001) who studied the impact of collisional dark matter on the formation of radial and giant arcs.

observations, Merten et al. (2011) find that Abell 2744 is a very complex merger. This is evident from their results shown in Figure 8. Two of the components strongly resemble the “Bullet cluster”, with a separation of  $17''$  between lensing and X-ray peaks in the core and a matching  $30''$  offset for the smaller Northern component. Following the approach of Markevitch et al. (2004) a dark matter self-interaction cross-section of  $\sigma/m < 3 \pm 1 \text{ cm}^2 \text{ g}^{-1}$  can be inferred.

Abell 2744 features another interesting structure: towards the North-West, two peaks are detected in the mass map, and one peak in the *Chandra* map, but they are all separated from each other and the nearest bright galaxies. In addition, Merten et al. (2011) report a further mass peak without ICM on the Western side. As an explanation of the formation of the “ghost”, “dark”, and “stripped” clumps, Merten et al. (2011) suggest a complicated merger scenario. In this picture, at least two merger events occurred almost simultaneously, involving up to four different substructures colliding with the core of Abell 2744.

Abell 520 is another example of a complicated merging system. Like 1ES 0657–558 it shows clear evidence of a shock in the X-ray observations. Using deep CFHT observations, Mahdavi et al. (2007) found a significant peak in the mass reconstruction that coincided with the peak of the X-ray emission, but where almost no cluster galaxies were present. This result was confirmed by Jee et al. (2012), using deep *HST* WFPC2 observations, although even deeper ACS observations by Clowe et al. (2012) do not show evidence of a peak. These interesting clusters highlight the importance of mass reconstructions as well as the combination of strong and weak lensing information, if available.

## 5 Cluster halo properties from weak lensing

In §6 we review applications of weak lensing to estimate the masses of clusters, and the subsequent comparison to baryonic tracers. In this section we discuss observational tests of two key predictions from numerical simulations of structure formation in a cold dark matter dominated universe. We first review constraints on the radial density profiles, which are predicted to be well described by Eqn. 28. In §5.2 we review measurements of the ellipticities of cluster halos, which can be compared to the CDM predictions.

To examine the density profiles at large radii, weak gravitational lensing is well suited, especially when combined with strong lensing studies. This is because the weak lensing signal can be measured out to large radii, thus probing the gravitational potential on large scales. Even if they were measurable, the results from most dynamical techniques would be difficult to interpret because the outskirts are not fully virialized. We note that it is possible to study the velocity field of the cluster infall region, which provides a direct measure of the escape velocity and thus the cluster mass. In practice this is done by identifying the caustics in redshift space (Diaferio & Geller 1997; Diaferio 1999). This technique has been applied to a number of local clusters of galaxies. Rines et al. (2003) and Diaferio et al. (2005) compared weak lensing estimates to the masses inferred from the identification of caustics in redshift space for three clusters and found good agreement on scales of  $\sim 2\text{Mpc}$ .

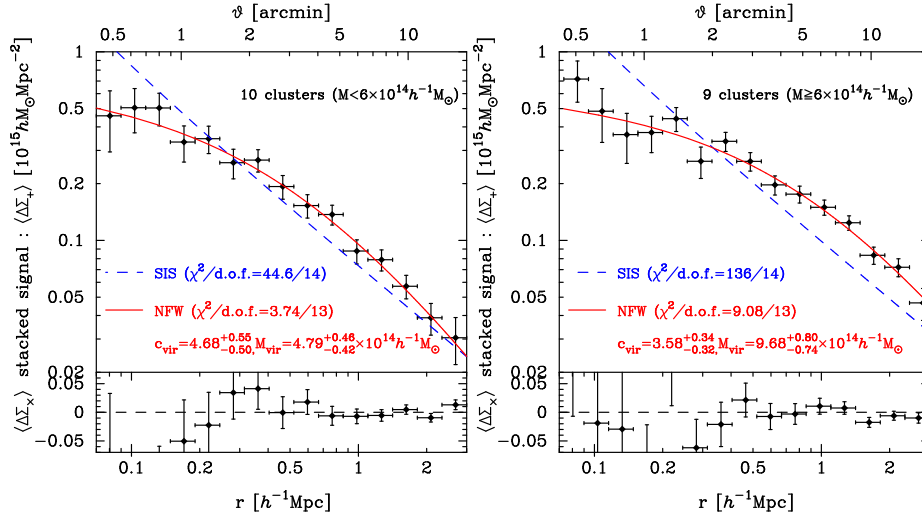


**Fig. 9** Stacked surface mass density contrast  $\langle \Delta \Sigma \rangle$  of 19 LoCuSS clusters. Points with error bars show the measured tangential shear signals of clusters below (left panel) and above (right panel) a mass of  $6 \times 10^{14} h^{-1} M_{\odot}$ . The solid red lines gives the best NFW fit, while the dashed blue lines gives the best SIS fit to the data. The lower sections of both panels show the corresponding stacked cross-components. Figure from Okabe et al. (2010).

### 5.1 Density Profiles

One of the most important quantities that can be inferred from weak lensing is the density profile of clusters. Although this can be measured for individual clusters, the mention of a radial profile implicitly assumes a high degree of spherical symmetry, which may not be appropriate. Furthermore cosmic noise reduces the precision when considering only weak lensing measurements (Hoekstra 2003). Hence, a better question to ask is what the average density profile of clusters looks like. Provided the selection of the cluster sample is not (too) sensitive to the orientation of the cluster, the ensemble averaged cluster should be rather spherical. These results can be directly compared to the predictions of  $N$ -body dark matter simulations.

Weak lensing studies of the density profile start with the tangential shear profile  $g_t(r)$ , which then can be converted into a projected density profile  $\kappa(r)$ . Strong lensing and combined methods typically yield the  $\kappa$  profile via the lensing potential. Alternatively one can fit a parametrized model to the tangential shear. The latter approach was used by Okabe et al. (2010) who studied the shear profiles of  $0.15 < z < 0.30$  clusters observed by LoCuSS.

Out of the 22 clusters that have color information (for background selection and dilution correction; see §3.2.2) and do not show a complex mass distribution, 19 are modelled well by an NFW fit (i.e. better than using an SIS fit). Stacking the shear signals of these 19 clusters, the projected density contrast was measured over a wide radial range ( $70 h^{-1} \text{kpc}$  to  $3 h^{-1} \text{Mpc}$ ; Fig. 9). Fitting to the stacked signals of the ten lower-mass<sup>3</sup> ( $M_{\text{vir}} < 6 \times 10^{14} h^{-1} M_{\odot}$ ) and higher-mass ( $M_{\text{vir}} \geq 6 \times 10^{14} h^{-1} M_{\odot}$ )

<sup>3</sup> Okabe et al. (2010) use a virialisation overdensity based on their adopted “concordance”  $\Lambda$ CDM cosmology,  $\Delta_{\text{vir}} \approx 112$  at  $z=0.2$ .

clusters, an NFW model is strongly favoured over an SIS model, given the noticeable curvature in the measured profile. Even at the largest tested cluster-centric separations, determined by the field-of-view of Subaru/SuprimeCam, the signal follows an NFW function. Matching expectations, the stacked lower-mass cluster signal follows a slightly more concentrated NFW profile than the higher-mass systems.

#### 5.1.1 Results from stacking

To average out the effects of the cluster large-scale structure stacking is clearly convenient. It also allows us to extend the range to much lower cluster masses and study their *statistical* properties. The stacking process has to be performed in a sensible way, meaning e.g. taking into account the redshift scaling of the signals from clusters within a (redshift) bin. Johnston et al. (2007a) developed the extraction of 3D density and mass profiles from stacked clusters and performed numerical simulations to test the performance.

Naturally, stacking methods are even more sensitive to miscentering errors than weak lensing studies of individual clusters. But this can be modeled (see §2.2) and the downside is outweighed by the cancellation of unrelated large-scale structure contaminants. Furthermore, the analysis tends to reduce additive errors in the shape analysis, because they do not contribute coherently, unless the clusters are targeted and always appear on the same position in the field-of-view.

The SDSS has made important contributions to the statistical studies of lenses, ranging from galaxies to clusters of galaxies. For example Mandelbaum et al. (2006) used the luminous red galaxy (LRG) sample to define a sample of galaxy groups and clusters of galaxies and fitted NFW models to the lensing signal  $\Delta\Sigma(r)$ . They found that the resulting concentrations agree well with  $\Lambda$ CDM predictions. Mandelbaum et al. (2006) also review extensively possible systematic effects. The mass range was extended to lower masses in Mandelbaum et al. (2008) who thus provided constraints on the concentration parameter over more than two orders of magnitude in mass ( $10^{12} - 5 \times 10^{14} M_{\odot}$ ).

Combining both spatial and color-space clustering with the presence of a BCG candidate (Koester et al. 2007), the lensing signal for the  $0.1 \leq z \leq 0.3$  MaxBCG cluster catalog was studied by Sheldon et al. (2009). The clusters were subdivided either by luminosity (see Figure 4) or by richness  $N_{200}$ . Sheldon et al. (2009) report significant  $\Delta\Sigma$  profiles in all tested richness and (total *i*-band) luminosity bins, spanning a scale between small galaxy groups and clusters. These measurements were analysed further by Johnston et al. (2007b) who fitted a halo model (as discussed in §2.2.2 and shown in Fig. 4). The excellent precision of the measurements enabled Johnston et al. (2007b) to determine the concentration as a function of halo mass, finding good agreement with previous estimates.

#### 5.1.2 Results for individual clusters

Although stacking analyses can provide excellent constraints on the average density profiles over a wide range in mass, it is nonetheless interesting to study individual systems, even if the results are limited by the large scale structure. The study of mass density profiles using gravitational lensing are discussed in detail by Meneghetti et al. (2012), but here we discuss briefly some recent results.

Zitrin et al. (2012) used 16 band *HST* imaging from the CLASH survey, as well as VLT/VIMOS spectroscopy to construct a strong lensing model for the massive  $z=0.44$  cluster MACS J1206–0847 based on 47 images of 12 background sources. The mass profile resulting from the strong lensing solution exhibits a slope of  $d \log \Sigma / d \log r = -0.55 \pm 0.10$ , measured over a range of  $5 \lesssim r \lesssim 300$  kpc, or out to about twice the Einstein radius. This is typical of a relaxed and rather concentrated cluster, and corroborates the notion of MACS J1206–0847 being relaxed, despite its unusually high X-ray luminosity and temperature.

Coe et al. (2012) determined the inner mass profile of Abell 2261, also as part of the CLASH survey. The *HST* imaging was combined with wide-field Subaru and KPNO observations. Combining strong and weak lensing, and also including gravitational magnification to break the mass-sheet degeneracy, the authors find the profiles from strong and weak lensing to agree well in the overlapping region (upper panel of Fig. 10). Both the breaking of the mass-sheet degeneracy and the careful selection of background galaxies using color information are important in achieving this agreement. The resulting mass profile is well represented by an NFW fit of moderate concentration ( $c_{\text{vir}} = 6.2 \pm 0.3$ ), contrasting earlier findings (e.g., Umetsu et al. 2009) of a concentration  $c_{\text{vir}} > 10$ . While Coe et al. (2012) find that the hydrostatic mass estimate based on their *Chandra* analysis agrees with the lensing mass profile at the cluster center, at  $r_{2500}$ , the outermost radius covered with *Chandra*, it is  $\sim 35\%$  lower than the lensing mass (lower panel of Fig. 10).

A 20% deviation from hydrostatic equilibrium is necessary to alleviate the discrepancy between the X-ray and lensing mass profiles. Although non-thermal pressure sources can at least partly explain the difference, halo elongation along the line of sight can reconcile the X-ray and lensing observations, as found by Coe et al. (2012): the agreement between profiles improves when a 2:1 axis ratio, consistent with expectations from simulated clusters, is assumed (cf. Fig. 10). We refer the reader to Limousin et al. (2012) in this volume for a review on this particular topic.

## 5.2 Shapes of Dark Matter Halos

An important prediction of numerical simulations of structure formation is that dark matter halos are triaxial, which complicates the comparison of weak lensing masses to other methods. This prediction can be studied using gravitational lensing. Strong lensing studies can be used to study the inner regions, although the interpretation of the results may be complicated by the presence of baryons.

The shape of the dark matter halo at larger radii can be studied using weak gravitational lensing. Although one could use mass reconstructions for this purpose, it is better to examine the effect of an elliptical mass distribution on the shear field. For instance, Hoekstra et al. (1998) looked at the azimuthal variation of the tangential shear around the cluster MS1358+62. They found that the cluster mass distribution was elongated with an axis ratio and position angle that agreed well with strong lensing results.

A more extensive study was carried out by Oguri et al. (2010) who analysed a subsample of the Local Cluster Substructure Survey (LoCuSS) sample observed with Subaru’s SuprimeCam. Oguri et al. (2010) fit an elliptical model (with a radial NFW model) to the 2D shear map of 25 clusters. Their fit accounts for covariance between the errors in the grid cells caused by cosmic noise. An example of one of the clusters in



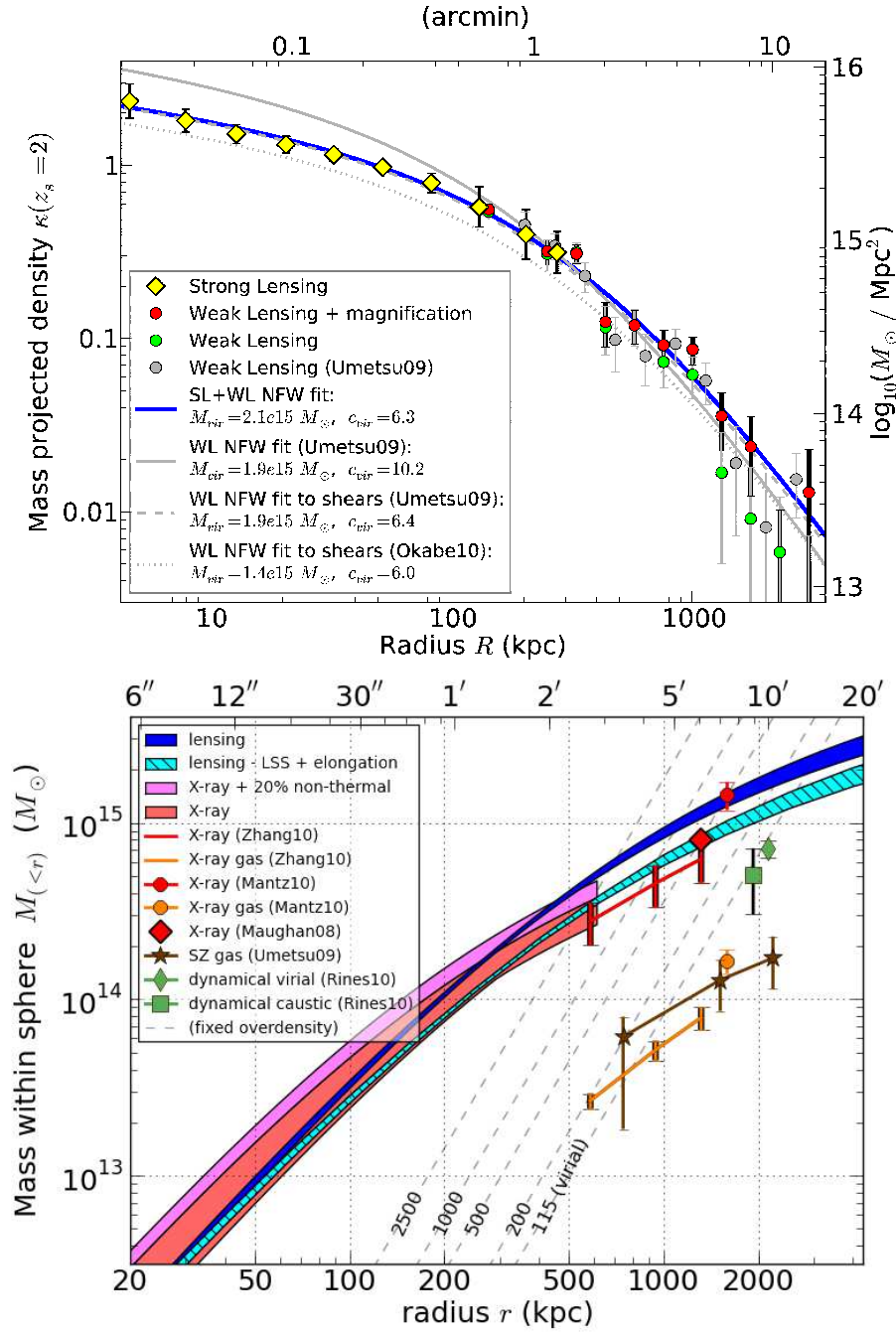


**Fig. 10** *Upper panel:* Projected mass density of Abell 2261. Shown are various strong and weak lensing constraints to the  $\kappa$  profile and the respective NFW fits (see legend). *Lower panel:* Mass profiles of Abell 2261. Shown are cluster masses within a sphere of radius  $r$  from a variety of observables (see legend). For comparison, dashed lines show fixed overdensities  $\Delta$ . Figures from Coe et al. (2012).

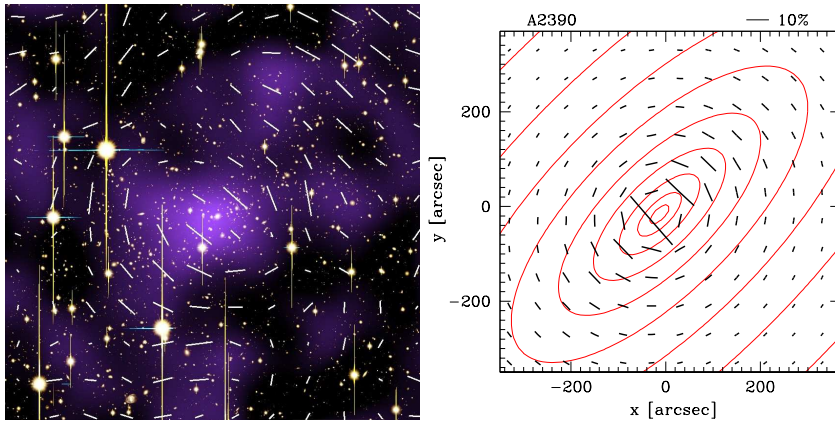


**Fig. 11** Shear field of Abell 2390. Sticks in both panels show the average shear measured in cells of  $1'$  mesh size. The measured field in the left panel has been smoothed by a Gaussian of  $\approx 1.6'$  FWHM. Also shown is the projected surface mass map, overlaid on the Subaru image. The right panel presents the shear field by the best-fitting elliptical NFW model. Figure from Oguri et al. (2010).

their sample is presented in Figure 11. For 18 out of their 25 clusters, the elliptical shear model proves to be a good fit. From these clusters, Oguri et al. (2010) obtain a mean halo ellipticity<sup>4</sup> of  $\langle e \rangle = 0.46 \pm 0.04$  (where the uncertainty is obtained via a Monte Carlo technique). This value is in good agreement with the prediction of  $\langle e \rangle = 0.42$  for simulated triaxial dark matter halos (e.g., Jing & Suto 2002).

Recently, Oguri et al. (2012) published a new measurement of the halo ellipticity, based on a combined strong/weak lensing study of 28 galaxy clusters selected from the Sloan Giant Arcs Survey. The combination of the strong and weak lensing data is performed using the Oguri et al. (2009) method. Using both an independent sample and a different technique, the authors find a mean halo ellipticity of  $\langle e \rangle = 0.47 \pm 0.06$ , confirming the results of Oguri et al. (2010), and in good agreement with  $\Lambda$ CDM expectations. Oguri et al. (2012) also detect a correlation of the halo ellipticity measured by lensing with the distribution of luminous ( $L \gtrsim L_*$ ) galaxies.

## 6 Cluster masses from weak lensing

There is an ongoing effort to use the observed number density of clusters of galaxies as a precision probe of cosmological parameters (see e.g., Allen et al. 2011, for a recent review). A correct interpretation of the observations relies on the ability to relate the observables to the mass. The calibration of such “scaling relations”, reviewed in detail by Giodini et al. (2012) in this volume, is still an important limiting factor for the precision of recent cluster surveys. Weak gravitational lensing masses, however, are playing an increasingly important role and we highlight a few results in this section.

One reason for the popularity of weak lensing is that the method is considered sufficiently mature, thanks to improved shape measurements as discussed in §3.1. Also important is the fact that the cluster lensing signal can be measured out to large radii.

<sup>4</sup> Here, the ellipticity of an ellipse with major and minor axes  $a$  and  $b$  is defined as  $e = 1 - b/a$ .

Finally, there is increasing evidence that non-gravitational processes such as AGN feedback play a role in cluster formation. Furthermore, pressure support by turbulent motion of the ICM leads to biases in the hydrostatic masses (e.g., Nagai et al. 2007; Mahdavi et al. 2008, 2012), which need to be calibrated observationally.

As weak lensing masses are insensitive to the dynamical state of the cluster, the results can be readily compared to cosmological numerical simulations. Note that this does not imply that weak lensing masses themselves are unbiased, only that the biases can be reliably quantified using numerical simulations. The main complication to compare lensing masses to other tracers is the fact that clusters are complicated three-dimensional structures. Although the measurement of the lensing signal itself does not require assumptions about the detailed geometry of the cluster, comparison to other observations or predictions does rely on the assumed geometry.

Several studies have examined the impact of this. For instance, Meneghetti et al. (2010) focused specifically on the comparison of lensing masses and X-ray estimates using hydrodynamical simulations. From this study it is clear that the triaxiality of the halo limits the usefulness of comparing results for individual systems, but large samples can provide key constraints on the gas physics in clusters. Note that it is possible to account for the triaxiality in the modeling by combining multi-wavelength data (see Limousin et al. 2012; Morandi & Limousin 2012). Alternatively, Corless & King (2008) and Corless et al. (2009) investigated the fitting of triaxial models to the shear field instead. They showed that this approach, using priors obtained from numerical simulations can indeed reduce the bias in the recovered weak lensing mass.

It has also become clear that the bias in the (deprojected) weak lensing mass depends on the methodology and the radial range that is used. For instance Becker & Kravtsov (2011) have shown that NFW model fits to the signal at large radii ( $> 10'$ ) biases the mass low by  $\sim 6\%$ , whereas the bias is smaller when the outer radius of the fit is limited to  $1 - 2r_{\text{vir}}$ . If left unaccounted for, this leads to a significant contribution to the systematic error budget for studies that contain 10 or more clusters. Large cluster surveys therefore need to compare the algorithm used to infer the mass to such simulations, as was done by High et al. (2012).

## 6.1 Results from stacking analyses

As discussed in §2.2 the signal-to-noise is too low for low mass systems, or clusters at high redshifts. By stacking of the lensing signal from an ensemble of objects we can nonetheless provide constraints on their (average) mass. This was first done for a sample of 50 galaxy groups from the CNOC2 field galaxy redshift survey in Hoekstra et al. (2001) who found fair agreement between the lensing and dynamical mass. Although extended by Parker et al. (2005) who studied of 116 groups, these studies were limited by the relatively small number of systems.

*SDSS*: As in so many areas of astronomy, the SDSS also has had a great impact in the study of cluster masses, in particular the low-mass end. The large survey area provides the opportunity to stack the signals of many clusters and study their mass as a function of binned baryonic properties. As discussed in §2.2.2 the resulting cluster-mass cross-correlation signal (shown in Figure 4) can be modeled, which in turn yields mass estimates for the various ensembles. The ensemble-averaged weak lensing signal and subsequent mass modelling were presented in Sheldon et al. (2009) and Johnston

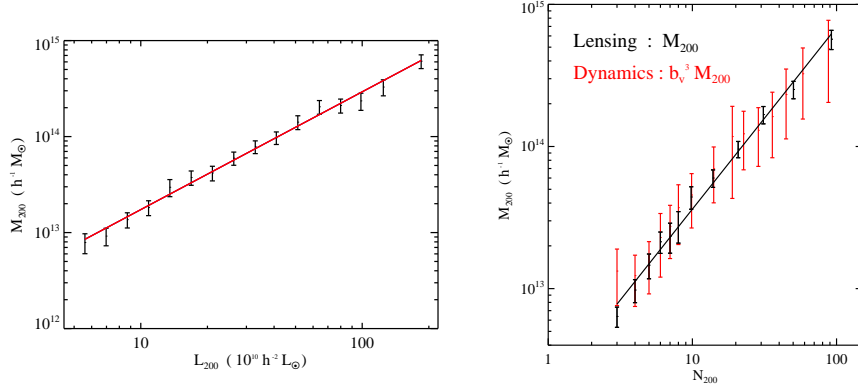


**Fig. 12** From Johnston et al. (2007b). *Left panel:* Lensing mass  $M_{200}$  as a function of the optical luminosity. *Right panel:* The black points show the best fit weak lensing mass  $M_{200}$  as a function of cluster richness  $N_{200}$ . The scaling relation is well described by a single power law with exponent  $\alpha = 1.28$ . The red points show the dynamical mass estimates from Becker et al. (2007), which agree well with the lensing masses.

et al. (2007b), respectively. The left panel of Figure 12 shows the resulting  $M_{200}$  as a function of the optical luminosity. The right panel of Figure 12 compares the mass to the cluster richness (quantified by  $N_{200}$ , the number of red-sequence galaxies within  $r_{200}$ ). Johnston et al. (2007b) also compared to the dynamical masses determined by Becker et al. (2007) and found good agreement *on average* (see the red points in Fig. 12. This suggests that the difference between the dark matter and galaxy velocity dispersions is fairly small. Finally, Rykoff et al. (2008) compared the SDSS lensing masses to stacked X-ray luminosity estimates from *ROSAT* All-Sky Survey data (also see Giodini et al. 2012).

*COSMOS:* Although the SDSS analyses have been able to provide excellent results for the group regime, the shallowness of the data limits the constraints to relatively low redshift. Furthermore, the low signal-to-noise ratio per system prevents efficient multi-wavelength studies. Such work is best done using deep high-quality data, which is not (yet) available for large areas. The COSMOS field of 1.64 square degrees has been studied extensively, and a wide range of data, including optical (*HST* and VLT) and X-ray (*XMM-Newton* and *Chandra*) observations, have been obtained. Leauthaud et al. (2010) used this data set to investigate the weak lensing properties of a sample of 206 X-ray-selected galaxy groups with  $0.2 < z < 0.9$  from Finoguenov et al. (2007). The source catalogue is based on earlier COSMOS results (Leauthaud et al. 2007).

Leauthaud et al. (2010) stack the shear signal in nine  $L_X$  bins and constrain the slope  $\alpha$  of the  $M_{200}^{\text{wl}}-L_X$  relation. The results are reproduced in Figure 13. While their COSMOS data alone yield  $\alpha = 0.66 \pm 0.14$ , a combination with earlier results tightens constraints to  $\alpha = 0.64 \pm 0.03$ , inconsistent with the self-similar prediction of  $\alpha = 0.75$ . Comparing to earlier studies of the  $M_{200}^{\text{wl}}-L_X$  relation for clusters, Leauthaud et al. (2010) find overall agreement within the error bars of their measurement (Fig. 13). The inclusion of group data improves the knowledge on the scaling relation, illustrating the

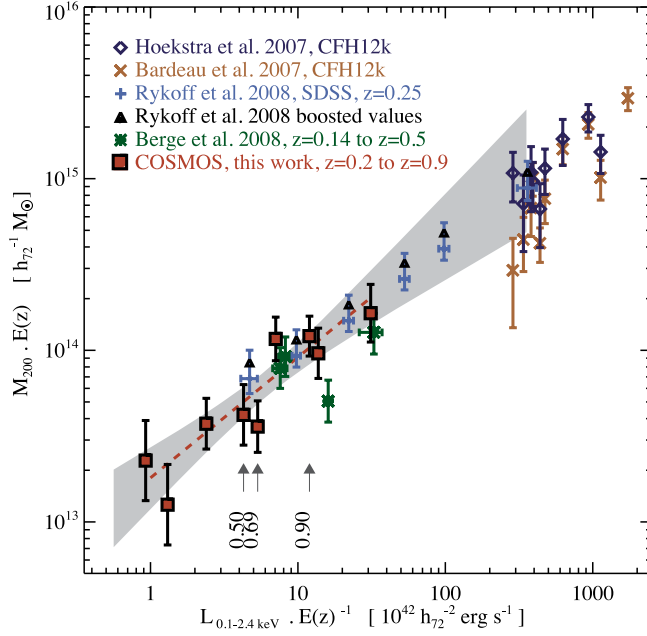


**Fig. 13** Figure from Leauthaud et al. (2010); Scaling relation between  $M^{\text{wl}}$  and  $L_X$ , comparing stacking results from COSMOS galaxy groups (Leauthaud et al. 2010, squares) with earlier results. Arrows point at the three highest redshift COSMOS bins. The grey area gives the 68% confidence regions of the scaling relation derived from the COSMOS data.

usefulness of weak lensing as a calibration tool to the next generation of X-ray cluster cosmology surveys (also see the comparison between results in Hoekstra et al. 2011a).

## 6.2 Recent studies of samples of individual clusters

The first weak lensing studies targeted massive clusters of galaxies in order to maximize the signal-to-noise. A number of clusters were studied in the '90s with relatively small cameras. Although these pioneering studies have proven critical to advance weak gravitational lensing to its current state, these masses do not meet the standards of current state-of-the-art analyses. Modern results are based on deep wide-field imaging data, and analysed using well-tested shape measurement algorithms (see e.g. §3.1). Consequently, we will limit the discussion in this section to only the most recent results that study ever larger samples of clusters.

Most of the recent increase in the number of clusters with individual weak lensing mass estimates has come from ground-based observations, but larger samples are also being studied using *HST*, such as the ongoing Cluster Lensing And Supernova survey with Hubble (CLASH). The most recent published large sample based on *HST* data, is the study by Jee et al. (2011) who presented weak lensing masses for a sample of 22 high-redshift ( $0.91 < z < 1.46$ ) clusters of galaxies. Unfortunately the large number of targets with deep imaging comes at the price of a relatively small field-of-view. As a result the masses have been derived from NFW fits to the observed tangential shear

profiles. Although one has little choice in this case, this may lead to biases because Jee et al. (2011) studied clusters that have only recently formed, and thus may show large deviations from a simple NFW model. Furthermore, the lack of photometric redshifts for the sources leads to additional uncertainties as discussed in §3.2.1. For the 15 clusters with X-ray temperature measurements Jee et al. (2011) find a power-law slope of  $1.54 \pm 0.23$  for the  $M - T_X$  relation, consistent with the self-similar value. However, compared to measurements at low redshift, the normalization is lower by 20 – 30%, suggesting some mild evolution.

The study of massive clusters using ground-based telescopes has also progressed tremendously in recent years, and here we will focus on the three largest studies. We mention briefly a number of other ongoing studies as well. Israel et al. (2012) presented results for an initial sample of 7 clusters drawn from the 400d galaxy cluster survey, with the final study targeting 36  $0.35 < z < 0.9$  clusters. High et al. (2012) presented masses for 5 clusters from the South Pole Telescope (SPT) survey, with a larger sample already observed. Foëx et al. (2012) presented results for a sample of 11 X-ray bright  $0.4 < z < 0.6$  clusters observed with MegaCam at CFHT. The large ground-based projects that we will review in more detail are the Local Cluster Substructure Survey (LoCuSS; Okabe et al. 2010; Zhang et al. 2010; Marrone et al. 2012), the Canadian Cluster Comparison Project (CCCP; Hoekstra 2007; Mahdavi et al. 2008; Hoekstra et al. 2012; Mahdavi et al. 2012) and the Weighing the Giants Project (WtG; von der Linden et al. 2012; Kelly et al. 2012; Applegate et al. 2012).

*LoCuSS:* Okabe et al. (2010) presented weak lensing masses for 29 clusters with  $0.15 < z < 0.3$  using deep Suprime-Cam data obtained with the Subaru telescope. This sample presents a subset of the full LoCuSS sample, which is a systematic multi-wavelength survey of X-ray luminous clusters of galaxies with  $L_X > 2 \times 10^{44}$  erg/s. Importantly, no further selection was made based on other physical properties. Results on the density profiles of clusters were already reviewed in §5.1.

Zhang et al. (2010) derived hydrostatic masses for 12 clusters using *XMM-Newton* observations, and compared these to the weak lensing masses. They find a good agreement, as opposed to Mahdavi et al. (2008) and Mahdavi et al. (2012). We note here that comparison to other lensing results suggest that the Okabe et al. (2010) masses are biased low (see discussion below). Although the sample is small, Zhang et al. (2010) find that the X-ray gas mass shows the least amount of scatter when compared to the weak lensing mass. A subset of 18 clusters was used by Marrone et al. (2012) to study the scaling relation between the SZ Compton parameter  $Y$  and weak lensing mass. They found an intrinsic scatter of 20% in the mass at fixed  $Y$ , with a suggestion of a dependence on morphology.

*CCCP:* The main aim of CCCP is to compare different baryonic tracers of cluster mass and to study the cluster-to-cluster variations in these relations. Weak lensing masses for an initial sample of 20 clusters, based on archival CFHT observations, were presented in Hoekstra (2007). This sample was augmented with masses for another 32 clusters in Hoekstra et al. (2012), based on CFHT Megacam observations that targeted 30 clusters. The final sample covers  $0.15 < z < 0.55$  with most of the clusters around  $z \sim 0.2$ , and thus overlapping partly with the sample studied by Okabe et al. (2010). Hoekstra et al. (2012) compare their aperture masses to SZ results from Bonamente et al. (2008) and Planck Collaboration et al. (2011), concluding that the SZ signal correlates well with

weak lensing mass. The intrinsic scatter that they measure is smaller but consistent with the results from Marrone et al. (2012).

The comparison with X-ray measurements is presented in Mahdavi et al. (2012). This work confirms the earlier finding by Mahdavi et al. (2008) that hydrostatic masses underestimate the weak lensing masses by  $\sim 10\%$  on average. Splitting the sample by central entropy suggests X-ray and lensing masses agree for low-entropy systems, whereas less relaxed clusters show a bias of  $15 - 20\%$ . In support of the finding by Zhang et al. (2010) for a sample of 12 clusters, Mahdavi et al. (2012) find very little scatter in the gas mass fractions, with the gas mass in fact being the most robust indicator of weak lensing mass. This is to be contrasted by claims based on numerical simulations that suggest that  $Y_X$ , the product of gas mass and X-ray temperature, is a better indicator (Kravtsov et al. 2006). Mahdavi et al. (2012) do note that the scatter in  $Y_X$  appears to be independent of dynamical state, which may be beneficial for cosmological studies with galaxy clusters.

*WiG:* Applegate et al. (2012) presented weak masses for 51 of the most X-ray luminous clusters currently known. Compared to LoCuSS and CCCP, this work includes a more detailed study of the contamination by cluster members (see §3.2.2) thanks to more extensive wavelength coverage, including 5-band photometry for 27 of the clusters. Applegate et al. (2012) also quantify the measurement bias using dedicated image simulations and develop a Bayesian framework to include the source redshift information. Together with the accompanying papers (von der Linden et al. 2012; Kelly et al. 2012) this work provides another step forward in weak lensing cluster lensing, which is particularly important for the study of high redshift clusters.

There is substantial overlap between the various cluster samples and this was used by Applegate et al. (2012) to compare results. They find that the mass estimates for the overlapping clusters correlate very well, but that the normalizations show significant variations. In particular the Okabe et al. (2010) masses are lower by 23%, whereas the CCCP masses are 12% lower than the Applegate et al. (2012) measurements. This may point to biases in the weak lensing signal itself, but differences in the subsequent steps of converting the signal into a mass may contribute as well. For instance differences in the assumed source redshift distributions, mass-concentration relations, fitting ranges, etc. all contribute at the several percent level. An important task for the near future is to better understand the impact of the choices one needs to make.

## 7 Halos of cluster members

Galaxy properties depend on their local environment. The morphology-density relation (Dressler 1980) represents a well-known example of this. In recent years large surveys, such as the SDSS have enabled much more detailed studies of correlations of galaxy properties. The cluster environment is rather hostile to infalling galaxies. An important actor in changing the galaxy properties is tidal stripping. For instance, Cayatte et al. (1990) found that the extent of the HI gas in the galaxies of the Virgo cluster decreases when the galaxies are closer to the cluster center.

Current studies have mostly focused on the baryonic aspects of the galaxies, but a less studied question is how the properties of the dark matter halos around galaxies change with environment. Simulations and observations (e.g. Hoekstra 2004) have shown that galaxies in the field are surrounded by extended dark matter halos. Tidal

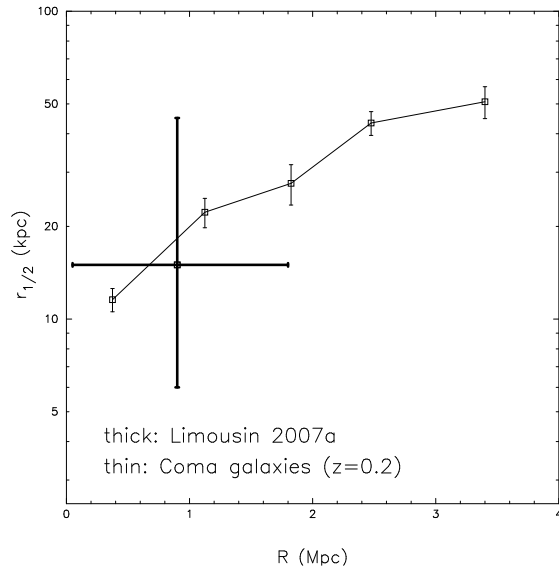


**Fig. 14** From Limousin et al. (2009): simulated half-mass radius of dark matter halos as a function of cluster-centric radius for a Coma-like cluster. The simulations show that halos are stripped as they are located near the cluster center. The thick data point with errors are derived from observations by Limousin et al. (2007) and in general agreement with the simulations.

stripping of these halos should occur when galaxies (both infalling and cluster members) interact with the gravitational tidal field of the cluster. The study of the lensing signal around cluster galaxies can provide unique constraints, and in this section we briefly review some of the (relatively few) results that have been obtained to date.

### 7.1 Comparison with numerical simulations

Cosmological numerical simulations suggests the presence of significant substructure in dark matter halos. In the case of galaxy scale halos these have not (yet) been detected; this has been referred to as the missing satellite problem (e.g. Klypin et al. 1999b). In the case of galaxy clusters these sub-halos correspond to the halos around cluster galaxies. Whether or not numerical simulations capture the formation of such halos is an important question which can be addressed using cluster galaxy-galaxy lensing studies. For instance, lack of numerical resolution can lead to premature destruction of simulated halos, a process known as over-merging (e.g. Klypin et al. 1999a).

These considerations suggest that predictions of the galaxy-galaxy lensing signal in clusters require high resolution simulations. Such a study was carried out by Limousin et al. (2009) who analysed hydrodynamical N-body simulations of galaxy clusters to probe tidal stripping of the dark matter subhalos. They investigated how the extent of the dark matter halos of cluster galaxies, quantified by the half mass radius  $r_{1/2}$ , depends on projected cluster-centric distance  $R$  and how it evolves as a function of redshift.



As shown in Figure 14, Limousin et al. (2009) find a clear trend for  $r_{1/2}$  with cluster-centric distance: the closer the galaxies are to the center of the cluster, the smaller the half mass radius. This trend is present for all redshifts that were studied (from  $z = 0$  to  $z = 0.7$ ). At the present day, galaxy halos in the central regions of clusters are found to be highly truncated, with the most compact having half mass radius of 10 kpc. The corresponding total mass of the cluster galaxies is also found to increase with projected cluster-centric distance and luminosity, but with more scatter than the trend of  $r_{1/2}$  with radius  $R$ . The thick data point in Figure 14 indicates the results of a comparison with galaxy-galaxy lensing results from Limousin et al. (2007) (also see below), indicating good agreement between the simulations and observations.

## 7.2 Results from cluster galaxy-galaxy lensing

The shear field generated by a galaxy cluster is dominated by the central halo, which is relatively smooth. However, when resolved with enough precision, local anisotropies due to the presence of cluster members can be discerned. Although the signal caused by a galaxy lens is typically small, the underlying cluster convergence boosts the lensing effect. As a result, a detailed modeling of strong lensing in galaxy clusters can provide interesting constraints, as well as clear examples of galaxy-galaxy lensing in clusters.

The more subtle deformation in the shapes of background galaxies produced by the cluster lenses can be measured as well. A complication is that the halo signal decreases  $\propto 1/r^2$  beyond the radius where the density profile is truncated. Hence it is important to be able to probe the lensing signal on very small scales. This is why the first measurements used *HST* observations. The study by Geiger & Schneider (1999) for the galaxy cluster Cl0939+4713 led to a detection of galaxy-galaxy lensing, but the field-of-view was too small to allow strong conclusions to be drawn about the mass distribution of the cluster galaxies. A series of studies by Natarajan et al. (1998, 2002a, 2002b, 2009) also used *HST* observations. In their analysis they included constraints from multiple images systems which boosts the precision of the measurements.

The *HST* studies are, however, typically confined to relatively small cluster-centric radii, because of the small field-of-view. The exception is the work by Natarajan et al. (2009) who used a large *HST* mosaic covering up to 5 Mpc from the center of Cl0024+16. As a result Natarajan et al. (2009) were able to probe the galaxy population in three radial bins and inferred a larger extent for the halos of galaxies located in the outskirts of the cluster (i.e. at a cluster-centric distance between 3 and 5 Mpc) compared to the galaxies in the core of the cluster (between 0 and 3 Mpc), in agreement with the expectation from numerical simulations.

Panoramic ground-based cameras, which have proven important for studies of cosmic shear and cluster mass determinations have led to ground-based constraints as well. Limousin et al. (2007) studied a sample of massive galaxy clusters observed using the CFH12K camera at CFHT, which allowed them to probe the cluster galaxy population out to a large radius ( $\sim 2$  Mpc). The results from Limousin et al. (2007) are reproduced in Figure 15. The measurements suggest small truncation radii  $r_{\text{cut}}$  for galaxies located in massive clusters, with half-mass radii typically less than 50 kpc. This is significantly smaller compared to results from studies of field galaxies (Fischer et al. 2000; McKay et al. 2001; Hoekstra et al. 2003; Hoekstra 2004), which suggest half-mass radii larger than 200 kpc for lenses of equivalent luminosity.

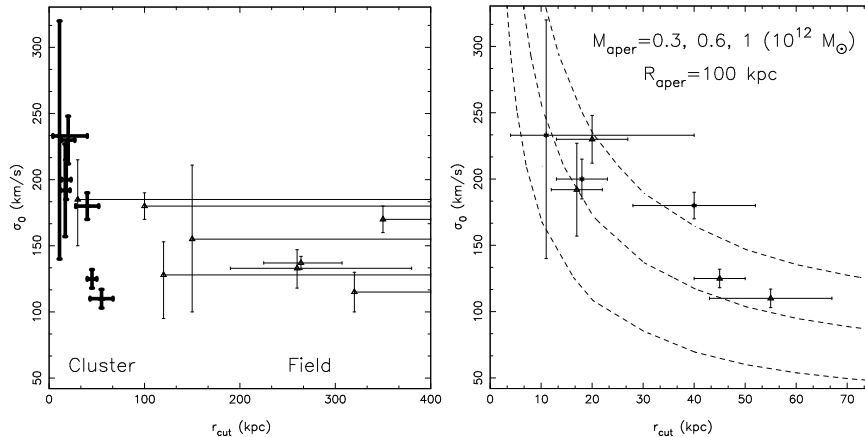


**Fig. 15** From Limousin et al. (2007). *Left panel:* Comparison of the cluster galaxy-galaxy lensing results (thick black points) to measurements of field galaxies (thin points). These results indicate that the halos around cluster galaxies are significantly smaller compared to galaxies in the field. *Right panel:* Zoom of the cluster results. Along the dotted lines the mass within a projected radius of  $R_{\text{aper}} = 100$  kpc is constant. The three curves correspond to the values indicated in the plot.

The overall finding of these pioneering studies is that dark matter halos in high density regions are stripped. The consequence is that observational constraints are difficult to obtain, because they require measurements very close to the lenses. Furthermore to study the sizes as a function of cluster-centric distance requires clean membership determination, because massive field galaxies can easily bias the results. The increased statistics from next generation surveys will improve the measurements, but in particular future space based projects, such as *Euclid*, that combine wide-field with high-resolution imaging, will provide a major step forward.

## 8 Conclusions & Outlook

Gravitational lensing studies of clusters of galaxies have gained more prominence in recent years. Strong lensing is now routinely observed in deep HST observations, providing a unique (magnified) view of the most distant galaxies, but also allowing a detailed modelling of the mass distribution in the central regions of clusters (see Meneghetti et al. 2012, for a more in-depth discussion of this application). In this review we focused on the determination of cluster masses, where weak gravitational lensing has become an important tool. As shown in §4, it allows for unique studies of the mass distribution in clusters of galaxies. The results reviewed in §6 demonstrate that weak lensing studies have become an important observational link between the results from numerical simulations and measurements from a number of baryonic tracers.

Cluster samples are increasing rapidly in size thanks to dedicated optical, SZ and X-ray surveys. Similarly the number of clusters for which weak lensing masses have been determined is increasing, with the most recent results presenting masses for several tens of clusters (Okabe et al. 2010; Hoekstra et al. 2012; Applegate et al. 2012).

Consequently, fewer results will be dominated by the statistical uncertainties caused by the intrinsic source ellipticity (although this cannot be avoided when considering individual systems). Observational systematics, such as the correction for the (anisotropic) smearing by the PSF which was discussed in §3.1, have largely been considered a problem for cosmic shear studies, but when considering a sample of  $\sim 100$  massive clusters the statistical errors are  $\sim 1\%$ , and thus quite comparable to the level needed and tested for cosmic shear. Cluster studies will, however, continue to benefit of further development in shape measurement techniques. Nonetheless a careful characterization of systematics is critical for current and future analyses.

For cluster studies, the dominant source of uncertainty remains the interpretation of the signal, which is complicated by the fact that clusters are neither round nor described by simple parametric density profiles. Comparison with numerical simulations indicate that weak lensing masses can be biased, but that the level depends on the details of the analysis. For instance, biases are small when NFW models are fit to the lensing signal within the virial radius. Masses derived from aperture masses may have smaller biases, which nonetheless need to be quantified. Finally, as discussed in §2.2.1, gravitational lensing is sensitive to all matter along the line-of-sight, which introduces another source of noise, which should be included when quoting the uncertainty in the mass measurement. This is particularly important when considering constraints on density profiles.

As reviewed in §3.2, ever since the first weak lensing studies of clusters has the limited knowledge of the source redshifts been a dominant source of bias. Thanks to deep, multi-wavelength, wide-angle surveys the average redshift distribution is now well established for ground based studies of intermediate redshift clusters. However, in the case of high-redshift ( $z \sim 1$ ) clusters, the lack of source redshift information is still a concern. This is a key regime for weak lensing studies, because those clusters are still dynamically young, and lensing masses are needed to calibrate other observables. It is possible to use distributions inferred from other, deep observations, but current data sets may not be sufficiently representative. Furthermore, the field-to-field variation increases the uncertainty in the mass measurement, which is already noisy due to the small number of galaxies behind the cluster.

None of these complications pose insurmountable problems for an increasingly more important role of weak gravitational lensing to study a range of properties of galaxy clusters. Furthermore, new questions can be addressed with more and better data. For instance the studies of the properties of dark matter halos in dense environments have to date been limited. These benefit from redshift information for the lenses to establish membership and from future space based observations that can probe the signal down to small radii. To conclude, the role of weak gravitational lensing in the study of galaxy clusters is increasing and thus the outlook for this area of research is positive, especially with the selection of the *Euclid* mission by ESA (Laureijs et al. 2011). This exciting project will provide a unique data set for the study the distribution of matter in clusters, using both strong and weak gravitational lensing.

**Acknowledgements** We would like to thank ISSI for their hospitality. HH acknowledges support from NWO Vidi grant 639.042.814 and Marie Curie IRG Grant 230924. We also thank Elisabetta Semboloni for a careful reading of this manuscript.

## References

- Abdelsalam H. M., Saha P., Williams L. L. R., 1998, *AJ*, 116, 1541
- Allen S. W., Evrard A. E., Mantz A. B., 2011, *ARA&A*, 49, 409
- Applegate D. E. et al., 2012, *ArXiv e-prints*
- Bacon D. J., Goldberg D. M., Rowe B. T. P., Taylor A. N., 2006, *MNRAS*, 365, 414
- Bahé Y. M., McCarthy I. G., King L. J., 2012, *MNRAS*, 421, 1073
- Bartelmann M., 1995, *A&A*, 299, 11
- Bartelmann M., 1996, *A&A*, 313, 697
- Bartelmann M., 2010, *Classical and Quantum Gravity*, 27, 233001
- Bartelmann M., Meneghetti M., et al., 2012, this volume
- Bartelmann M., Narayan R., Seitz S., Schneider P., 1996, *ApJ*, 464, L115
- Bartelmann M., Schneider P., 2001, *Phys. Rep.*, 340, 291
- Bauer A. H., Baltay C., Ellman N., Jerke J., Rabinowitz D., Scalzo R., 2012, *ApJ*, 749, 56
- Becker M. R., Kravtsov A. V., 2011, *ApJ*, 740, 25
- Becker M. R. et al., 2007, *ApJ*, 669, 905
- Bernstein G. M., 2010, *MNRAS*, 406, 2793
- Bildfell C., Hoekstra H., Babul A., Mahdavi A., 2008, *MNRAS*, 389, 1637
- Bonamente M., Joy M., LaRoque S. J., Carlstrom J. E., Nagai D., Marrone D. P., 2008, *ApJ*, 675, 106
- Bradač M. et al., 2006, *ApJ*, 652, 937
- Bradač M., Schneider P., Lombardi M., Erben T., 2005, *A&A*, 437, 39
- Brainerd T. G., Blandford R. D., Smail I., 1996, *ApJ*, 466, 623
- Bridle S. et al., 2010, *MNRAS*, 405, 2044
- Broadhurst T., Takada M., Umetsu K., Kong X., Arimoto N., Chiba M., Futamase T., 2005, *ApJ*, 619, L143
- Broadhurst T. J., Taylor A. N., Peacock J. A., 1995, *ApJ*, 438, 49
- Bryan G. L., Norman M. L., 1998, *ApJ*, 495, 80
- Cacciato M., Bartelmann M., Meneghetti M., Moscardini L., 2006, *A&A*, 458, 349
- Cayatte V., van Gorkom J. H., Balkowski C., Kotanyi C., 1990, *AJ*, 100, 604
- Clowe D., Bradač M., Gonzalez A. H., Markevitch M., Randall S. W., Jones C., Zaritsky D., 2006a, *ApJ*, 648, L109
- Clowe D., Bradač M., Gonzalez A. H., Markevitch M., Randall S. W., Jones C., Zaritsky D., 2006b, *ApJ*, 648, L109
- Clowe D., De Lucia G., King L., 2004a, *MNRAS*, 350, 1038
- Clowe D., Gonzalez A., Markevitch M., 2004b, *ApJ*, 604, 596
- Clowe D., Luppino G. A., Kaiser N., Henry J. P., Gioia I. M., 1998, *ApJ*, 497, L61
- Clowe D., Markevitch M., Bradač M., Gonzalez A. H., Chung S. M., Massey R., Zaritsky D., 2012, *ApJ*, 758, 128
- Coe D., Benítez N., Sánchez S. F., Jee M., Bouwens R., Ford H., 2006, *AJ*, 132, 926
- Coe D. et al., 2012, *ArXiv e-prints*
- Corless V. L., King L. J., 2007, *MNRAS*, 380, 149
- Corless V. L., King L. J., 2008, *MNRAS*, 390, 997
- Corless V. L., King L. J., Clowe D., 2009, *MNRAS*, 393, 1235
- Dawson W. A. et al., 2011, *ArXiv:1110.4391*
- de Putter R., White M., 2005, *New Astronomy*, 10, 676
- Diaferio A., 1999, *MNRAS*, 309, 610
- Diaferio A., Geller M. J., 1997, *ApJ*, 481, 633
- Diaferio A., Geller M. J., Rines K. J., 2005, *ApJ*, 628, L97
- Diego J. M., Tegmark M., Protopapas P., Sandvik H. B., 2007, *MNRAS*, 375, 958
- Dodelson S., 2004, *Phys. Rev. D*, 70, 023008
- Dressler A., 1980, *ApJ*, 236, 351
- Duffy A. R., Schaye J., Kay S. T., Dalla Vecchia C., Battye R. A., Booth C. M., 2010, *MNRAS*, 405, 2161
- Erben T., Van Waerbeke L., Bertin E., Mellier Y., Schneider P., 2001, *A&A*, 366, 717
- Finoguenov A. et al., 2007, *ApJS*, 172, 182
- Fischer P. et al., 2000, *AJ*, 120, 1198
- Föex G., Soucail G., Pointecouteau E., Arnaud M., Limousin M., Pratt G. W., 2012, *A&A*, 546, A106
- Ford J. et al., 2012, *ApJ*, 754, 143

- 
- Geiger B., Schneider P., 1999, MNRAS, 302, 118  
 Giodini S., Lovisari L., et al., 2012, this volume  
 Goldberg D. M., Bacon D. J., 2005, ApJ, 619, 741  
 Goldberg D. M., Natarajan P., 2002, ApJ, 564, 65  
 Golse G., Kneib J.-P., Soucail G., 2002, A&A, 387, 788  
 Gorenstein M. V., Shapiro I. I., Falco E. E., 1988, ApJ, 327, 693  
 Guzik J., Seljak U., 2002, MNRAS, 335, 311  
 Heymans C. et al., 2006, MNRAS, 368, 1323  
 Heymans C. et al., 2012, ArXiv e-prints  
 High F. W. et al., 2012, ArXiv e-prints  
 Hildebrandt H. et al., 2012, MNRAS, 421, 2355  
 Hildebrandt H. et al., 2011, ApJ, 733, L30  
 Hildebrandt H., van Waerbeke L., Erben T., 2009, A&A, 507, 683  
 Hirata C. M., Seljak U., 2004, Phys. Rev. D, 70, 063526  
 Hoekstra H., 2001, A&A, 370, 743  
 Hoekstra H., 2003, MNRAS, 339, 1155  
 Hoekstra H., 2004, MNRAS, 347, 1337  
 Hoekstra H., 2007, MNRAS, 379, 317  
 Hoekstra H., Donahue M., Conselice C. J., McNamara B. R., Voit G. M., 2011a, ApJ, 726, 48  
 Hoekstra H., Franx M., Kuijken K., 2000, ApJ, 532, 88  
 Hoekstra H., Franx M., Kuijken K., Carlberg R. G., Yee H. K. C., 2003, MNRAS, 340, 609  
 Hoekstra H. et al., 2001, ApJ, 548, L5  
 Hoekstra H., Franx M., Kuijken K., Squires G., 1998, ApJ, 504, 636  
 Hoekstra H., Franx M., Kuijken K., van Dokkum P. G., 2002a, MNRAS, 333, 911  
 Hoekstra H., Hartlap J., Hilbert S., van Uitert E., 2011b, MNRAS, 412, 2095  
 Hoekstra H., Jain B., 2008, Annual Review of Nuclear and Particle Science, 58, 99  
 Hoekstra H., Mahdavi A., Babul A., Bildfell C., 2012, ArXiv e-prints  
 Hoekstra H., Yee H. K. C., Gladders M. D., Barrientos L. F., Hall P. B., Infante L., 2002b, ApJ, 572, 55  
 Ilbert O. et al., 2006, A&A, 457, 841  
 Ilbert O. et al., 2009, ApJ, 690, 1236  
 Irwin J., Shmakova M., 2005, New Astronomy Reviews, 49, 83  
 Israel H. et al., 2010, A&A, 520, A58  
 Israel H., Erben T., Reiprich T. H., Vikhlinin A., Sarazin C. L., Schneider P., 2012, A&A, 546, A79  
 Jain B., Taylor A., 2003, Physical Review Letters, 91, 141302  
 Jee M. J. et al., 2011, ApJ, 737, 59  
 Jee M. J., Mahdavi A., Hoekstra H., Babul A., Dalcanton J. J., Carroll P., Capak P., 2012, ApJ, 747, 96  
 Jing Y. P., Suto Y., 2002, ApJ, 574, 538  
 Joachimi B., Mandelbaum R., Abdalla F. B., Bridle S. L., 2011, A&A, 527, A26  
 Johnston D. E., Sheldon E. S., Tasitsiomi A., Frieman J. A., Wechsler R. H., McKay T. A., 2007a, ApJ, 656, 27  
 Johnston D. E. et al., 2007b, ArXiv e-prints  
 Jullo E., Kneib J.-P., Limousin M., Elíasdóttir Á., Marshall P. J., Verdugo T., 2007, New Journal of Physics, 9, 447  
 Jullo E., Natarajan P., Kneib J.-P., D'Aloisio A., Limousin M., Richard J., Schimd C., 2010, Science, 329, 924  
 Kaiser N., Squires G., 1993, ApJ, 404, 441  
 Kaiser N., Squires G., Broadhurst T., 1995, ApJ, 449, 460  
 Kelly P. L. et al., 2012, ArXiv e-prints  
 Kitching T. D. et al., 2012, MNRAS, 423, 3163  
 Klypin A., Gottlöber S., Kravtsov A. V., Khokhlov A. M., 1999a, ApJ, 516, 530  
 Klypin A., Kravtsov A. V., Valenzuela O., Prada F., 1999b, ApJ, 522, 82  
 Kneib J.-P., Ellis R. S., Smail I., Couch W. J., Sharples R. M., 1996, ApJ, 471, 643  
 Koester B. P. et al., 2007, ApJ, 660, 239  
 Kravtsov A. V., Vikhlinin A., Nagai D., 2006, ApJ, 650, 128  
 Kuijken K., 1999, A&A, 352, 355  
 Kuijken K., 2008, A&A, 482, 1053  
 Laureijs R. et al., 2011, ArXiv e-prints

- 
- Leauthaud A. et al., 2010, *ApJ*, 709, 97  
 Leauthaud A. et al., 2007, *ApJS*, 172, 219  
 Leonard A., Goldberg D. M., Haaga J. L., Massey R., 2007, *ApJ*, 666, 51  
 Leonard A., King L. J., 2010, *MNRAS*, 405, 1854  
 Limousin M. et al., 2010, *MNRAS*, 405, 777  
 Limousin M., Kneib J. P., Bardeau S., Natarajan P., Czoske O., Smail I., Ebeling H., Smith G. P., 2007, *A&A*, 461, 881  
 Limousin M., Morandi A., Sereno M., Meneghetti M., Ettori S., Bartelmann M., Verdugo T., 2012, *ArXiv e-prints*  
 Limousin M., Sommer-Larsen J., Natarajan P., Milvang-Jensen B., 2009, *ApJ*, 696, 1771  
 Luppino G. A., Kaiser N., 1997, *ApJ*, 475, 20  
 Mahdavi A., Hoekstra H., Babul A., Balam D. D., Capak P. L., 2007, *ApJ*, 668, 806  
 Mahdavi A., Hoekstra H., Babul A., Bildfell C., Jeltama T., Henry J. P., 2012, *ArXiv e-prints*  
 Mahdavi A., Hoekstra H., Babul A., Henry J. P., 2008, *MNRAS*, 384, 1567  
 Mandelbaum R., Hirata C. M., Ishak M., Seljak U., Brinkmann J., 2006, *MNRAS*, 367, 611  
 Mandelbaum R. et al., 2005, *MNRAS*, 361, 1287  
 Mandelbaum R., Seljak U., Hirata C. M., 2008, *JCAP*, 8, 6  
 Marian L., Smith R. E., Bernstein G. M., 2010, *ApJ*, 709, 286  
 Markevitch M., Gonzalez A. H., Clowe D., Vikhlinin A., Forman W., Jones C., Murray S., Tucker W., 2004, *ApJ*, 606, 819  
 Marrone D. P. et al., 2012, *ApJ*, 754, 119  
 Massey R. et al., 2007, *MNRAS*, 376, 13  
 Massey R. et al., 2012, *ArXiv e-prints*  
 McKay T. A. et al., 2001, *ArXiv Astrophysics e-prints*  
 Medezinski E., Broadhurst T., Umetsu K., Oguri M., Rephaeli Y., Benítez N., 2010, *MNRAS*, 405, 257  
 Melchior P., Viola M., 2012, *MNRAS*, 424, 2757  
 Melchior P., Viola M., Schäfer B. M., Bartelmann M., 2011, *MNRAS*, 412, 1552  
 Meneghetti M., Bartelmann M., et al., 2012, this volume  
 Meneghetti M., Rasia E., Merten J., Bellagamba F., Ettori S., Mazzotta P., Dolag K., Marri S., 2010, *A&A*, 514, A93  
 Meneghetti M., Yoshida N., Bartelmann M., Moscardini L., Springel V., Tormen G., White S. D. M., 2001, *MNRAS*, 325, 435  
 Merten J., Cacciato M., Meneghetti M., Mignone C., Bartelmann M., 2009, *A&A*, 500, 681  
 Merten J. et al., 2011, *MNRAS*, 417, 333  
 Metzler C. A., White M., Loken C., 2001, *ApJ*, 547, 560  
 Miller L. et al., 2012, *ArXiv e-prints*  
 Miller L., Kitching T. D., Heymans C., Heavens A. F., van Waerbeke L., 2007, *MNRAS*, 382, 315  
 Miralda-Escude J., 1991, *ApJ*, 370, 1  
 Morandi A., Limousin M., 2012, *MNRAS*, 421, 3147  
 Nagai D., Vikhlinin A., Kravtsov A. V., 2007, *ApJ*, 655, 98  
 Natarajan P., Kneib J.-P., Smail I., 2002a, *ApJ*, 580, L11  
 Natarajan P., Kneib J.-P., Smail I., Ellis R. S., 1998, *ApJ*, 499, 600  
 Natarajan P., Kneib J.-P., Smail I., Treu T., Ellis R., Moran S., Limousin M., Czoske O., 2009, *ApJ*, 693, 970  
 Natarajan P., Loeb A., Kneib J.-P., Smail I., 2002b, *ApJ*, 580, L17  
 Navarro J. F., Frenk C. S., White S. D. M., 1997, *ApJ*, 490, 493  
 Oguri M., Bayliss M. B., Dahle H., Sharon K., Gladders M. D., Natarajan P., Hennawi J. F., Koester B. P., 2012, *MNRAS*, 420, 3213  
 Oguri M. et al., 2009, *ApJ*, 699, 1038  
 Oguri M., Takada M., Okabe N., Smith G. P., 2010, *MNRAS*, 405, 2215  
 Okabe N., Takada M., Umetsu K., Futamase T., Smith G. P., 2010, *PASJ*, 62, 811  
 Okura Y., Umetsu K., Futamase T., 2008, *ApJ*, 680, 1  
 Parker L. C., Hudson M. J., Carlberg R. G., Hoekstra H., 2005, *ApJ*, 634, 806  
 Pedersen K., Dahle H., 2007, *ApJ*, 667, 26  
 Planck Collaboration et al., 2011, *A&A*, 536, A8  
 Postman M. et al., 2012, *ApJS*, 199, 25  
 Pracy M. B., De Propris R., Driver S. P., Couch W. J., Nulsen P. E. J., 2004, *MNRAS*, 352, 1135

- 
- Rasia E. et al., 2012, *New Journal of Physics*, 14, 055018
- Refregier A., Bacon D., 2003, *MNRAS*, 338, 48
- Refregier A., Kacprzak T., Amara A., Bridle S., Rowe B., 2012, *MNRAS*, 425, 1951
- Rines K., Geller M. J., Kurtz M. J., Diaferio A., 2003, *AJ*, 126, 2152
- Rykoff E. S. et al., 2008, *MNRAS*, 387, L28
- Schmidt F., Leauthaud A., Massey R., Rhodes J., George M. R., Koekemoer A. M., Finoguenov A., Tanaka M., 2012, *ApJ*, 744, L22
- Schneider M. D., Bridle S., 2010, *MNRAS*, 402, 2127
- Schneider P., 2006, in *Saas-Fee Advanced Course 33: Gravitational Lensing: Strong, Weak and Micro*, G. Meylan, P. Jetzer, P. North, P. Schneider, C. S. Kochanek, & J. Wambsganss, ed., pp. 269–451
- Schrabback T. et al., 2010, *A&A*, 516, A63
- Seitz C., Schneider P., 1995, *A&A*, 297, 287
- Seitz C., Schneider P., 1997, *A&A*, 318, 687
- Seitz S., Schneider P., 1996, *A&A*, 305, 383
- Seitz S., Schneider P., 2001, *A&A*, 374, 740
- Seitz S., Schneider P., Bartelmann M., 1998, *A&A*, 337, 325
- Seljak U., 2000, *MNRAS*, 318, 203
- Semboloni E., Hoekstra H., Schaye J., van Daalen M. P., McCarthy I. G., 2011, *MNRAS*, 417, 2020
- Sheldon E. S. et al., 2009, *ApJ*, 703, 2217
- Simon P. et al., 2012, *MNRAS*, 419, 998
- Soucail G., Fort B., Mellier Y., Picat J. P., 1987, *A&A*, 172, L14
- Springel V., Farrar G. R., 2007, *MNRAS*, 380, 911
- Squires G., Kaiser N., 1996, *ApJ*, 473, 65
- Taylor A. N. et al., 2004, *MNRAS*, 353, 1176
- Taylor J. E. et al., 2012, *ApJ*, 749, 127
- Tyson J. A., Wenk R. A., Valdes F., 1990, *ApJ*, 349, L1
- Umetsu K. et al., 2009, *ApJ*, 694, 1643
- Umetsu K., Broadhurst T., Zitrin A., Medezinski E., Hsu L.-Y., 2011, *ApJ*, 729, 127
- Umetsu K. et al., 2012, *ApJ*, 755, 56
- van Uitert E., Hoekstra H., Schrabback T., Gilbank D. G., Gladders M. D., Yee H. K. C., 2012, *A&A*, 545, A71
- van Uitert E., Hoekstra H., Velander M., Gilbank D. G., Gladders M. D., Yee H. K. C., 2011, *A&A*, 534, A14
- von der Linden A. et al., 2012, *ArXiv e-prints*
- Walsh D., Carswell R. F., Weymann R. J., 1979, *Nature*, 279, 381
- Wittman D., Margoniner V. E., Tyson J. A., Cohen J. G., Becker A. C., Dell’Antonio I. P., 2003, *ApJ*, 597, 218
- Wright C. O., Brainerd T. G., 2000, *ApJ*, 534, 34
- Zhang Y.-Y. et al., 2010, *ApJ*, 711, 1033
- Zieser B., Bartelmann M., 2012, *ArXiv e-prints*
- Zitrin A. et al., 2012, *ApJ*, 749, 97
- Zwicky F., 1937, *ApJ*, 86, 217